SLAC–PUB–6384
November 1993
(T/E)

Tests of the Electroweak Standard Model at High Energies ($\sqrt{s} > 50$ GeV)*

Morris L. Swartz

Stanford Linear Accelerator Center
Stanford University, Stanford, CA 94309

Invited talk presented at the 16^{th} International Symposium on Lepton and Photon Interactions, Cornell University, Ithaca, NY, August 10–15, 1993

$\star$ Work supported by Department of Energy contract DE–AC03–76SF00515.

1. Preface

The Minimal Electroweak Standard Model (MSM) has been a remarkably successful description of a great variety of experimental phenomena. Constructed to incorporate quantum electrodynamics and the effective four-fermion (V-A) description of the weak charged current, the MSM correctly predicted the existence of the weak neutral current and has accurately described it from the eV scale to the 100 GeV scale. The successes of the MSM have been so impressive that few in our community would doubt that electroweak phenomena at the 100 GeV mass scale exhibit the features of a spontaneously broken, SU(2)×U(1) gauge symmetry.

Nevertheless, few in the theoretical particle physics community believe that MSM is a fully satisfactory and complete description of nature. The theory contains many arbitrary parameters to describe the fermion mass sector. The Higgs sector of the MSM is entirely *ad-hoc* and leads to a number of serious theoretical problems that plague theories with fundamental scalars.[1]

Unfortunately, few in the experimental particle physics community share the view that is so widely held by our theoretical colleagues. As empiricists, we tend to believe what we see and what we have seen is pure success. This has lead to an extremely dangerous mindset within the experimental half of the community, *that the MSM is Correct!* The average experimentalist really believes that an accurate measurement of an electroweak observable is equivalent to a measurement of the top quark mass.

I would like to remind this segment of the community that until quite recently, all tests of the MSM have been sensitive to the tree-level structure of the gauge boson and fermion sectors of the theory, the light particle content of the theory, and the running of the electromagnetic coupling constant due to light particle loops. We are just now achieving the sensitivity required to see heavy particle loops, purely weak radiative corrections, and three-gauge boson interactions. Deviations from the MSM may soon appear! Since we are entering a new regime of sensitivity, it is very important to discard all notions that the *MSM is correct*. All new results must be examined critically: those that appear to deviate from the MSM, AND those that appear to confirm it. It is the mission of all those working on precision tests of the MSM to prove it wrong, not to prove it right.

Table I

The physical parameters which specify the electroweak Standard Model.

Parameter	Tree-Level Expression	Measured Value	Precision
α_{em}	$gg'/4\pi(g^2+g'^2)$	$[137.0359895(61)]^{-1}$	4.5×10^{-8}
G_F	$[\langle\phi\rangle_0^2\sqrt{8}]^{-1}$	$1.16637(2)\times10^{-5}$ GeV^{-2}	1.7×10^{-5}
M_Z	$[(g^2+g'^2)\langle\phi\rangle_0^2/2]^{1/2}$	91.187(7) GeV	7.7×10^{-5}

2. Specification of the MSM

At tree-level, all low energy ($\sqrt{s} \lesssim 100$ GeV) electroweak phenomena depend on three parameters: the SU(2) coupling constant g, the U(1) coupling constant g', and the vacuum expectation value of the Higgs field $\langle\phi\rangle_0$. Since these parameters are not measured directly, they must be determined from the measured values of a set of three related physical parameters. In practice, most electroweak renormalization schemes are based on a physical parameter set. The conventional choice of the physical parameter set is: the electromagnetic fine structure constant α_{em}, the Fermi coupling constant G_F, and the mass of the Z boson M_Z. The current values of these parameters and their tree-level MSM expressions are listed in Table I. The current value of α_{em} is extracted from the remarkably precise measurements and QED calculations of the anomalous magnetic moment of the electron.[2] The Fermi coupling constant is extracted from precise measurements of muon lifetime.[3] The Z mass is a recent measurement by the LEP Collaborations and the Working Group on LEP Energy.[4]

Note that the physical parameters are measured at very different energy scales. In order to carry out loop-level calculations, it is necessary to evolve the low-energy parameters to the M_Z scale. The evolved value of α_{em} (due to known physics only) is calculated via a dispersion integral approach to be[5]

$$\alpha(M_Z^2) = [128.8 \pm 0.12]^{-1}. \tag{1}$$

The uncertainty on $\alpha(M_Z^2)$ is the dominant theoretical error on all electroweak calculations. It is due to the uncertainty on the measured cross section for $e^+e^- \to$ hadrons at low energies ($\sqrt{s} \lesssim 1$ GeV) which is used in the dispersion integral.

2.1 M_Z Measurement

The recent measurement of M_Z by the LEP Collaborations[4] is based on a scan of the Z lineshape that was performed in 1991. The 1991 energy scan featured the use of resonant depolarization to monitor the beam energy. This improved the knowledge of the energy scale of the machine by nearly a factor of three over the previously published result.

In an electron-positron storage ring, the number of spin precessions per orbit (the spin tune ν_s) is related to the beam energy E_{beam} by the following expression:

$$E_{beam} = \frac{m_e}{(g-2)/2} \cdot \nu_s = 0.4406486(1)\ \text{GeV} \cdot \nu_s, \tag{2}$$

where m_e and $(g-2)/2$ are the mass and anomalous magnetic moment of the electron, respectively. To measure the spin tune, the machine was operated at a center of mass energy (E_{cm}) of 93 GeV at which it was possible to develop transverse beam polarization. The spin tune was measured by creating an artificial spin resonance by perturbing the beam with pulsed horizontal magnets. In practice, one varies the frequency of pulsed magnets until the beam polarization vanishes. This depolarization frequency f_{dep} is related to the spin tune by the following expression:

$$f_{dep} = (\nu_s - \text{int}(\nu_s) \cdot f_{rev}, \tag{3}$$

where f_{rev} is the revolution frequency of the electron bunches along the nominal orbit, 11245.50(4) Hz.

The resonant beam depolarization measurements are plotted as corrections to the beam energy determined from flux loop measurements of a reference dipole magnet in Fig. 1. The results of proton beam and flux loop calibrations are also shown. The dotted lines show the previous and current uncertainties on the energy scale. Note that the previous uncertainty was dominated by the uncertainty on the magnet excitation curves which were needed to scale the lower-energy proton calibrations to the operational energy of the machine. The energy scale of the machine was established with a precision ΔE_{abs} of ± 5.4 MeV at $E_{cm} = 93$ GeV. The various contributions to this uncertainty are listed in Table II.

The uncertainties on the actual scan-point energies E_i are given by the following expression:

$$\frac{\Delta E_i}{E_i} = \frac{\Delta E_{abs}}{93\ \text{GeV}} \oplus \frac{|93\ \text{GeV} - E_i|}{E_i} \Delta E^{non-lin} \oplus \left(\frac{\Delta E}{E}\right)_i^{set} \oplus \frac{1}{\sqrt{n_i}} \left(\frac{\Delta E}{E}\right)_i^{rep}, \tag{4}$$

where $\Delta E^{non-lin}$ is the 1.5 MeV uncertainty in the scaling of LEP dipoles from 93 GeV to the operational energies, $(\Delta E/E)_i^{set}$ is the $3{\times}10^{-5}$ error on the setting

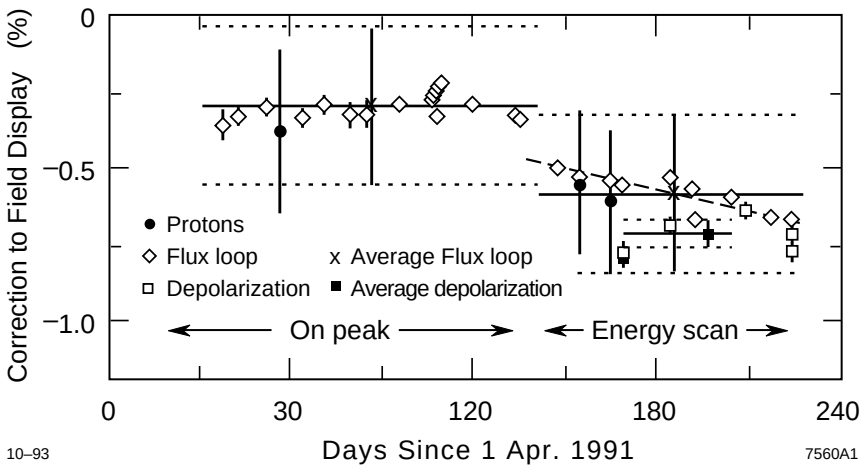

Figure 1. Proton, flux loop, and resonant depolarization measurements of the LEP beam energy are plotted as corrections to the energy determined by flux loop measurements of a reference dipole magnet.[4]

Table II

The components of the uncertainty on the LEP energy scale[4] at $E_{cm} = 93$ GeV.

Source of Uncertainty	Uncertainty
Spread in depolarization measurements	3.7 MeV
Temperature effects in dipoles	3.0 MeV
Slope in flux loop measurements	2.0 MeV
Reproducibility of operational parameters	1.0 MeV
ΔE_{abs} at $E_{cm} = 93$ GeV	5.3 MeV

of a scan point energy due to variations in the orbit and machine parameters, n_i is the number of fills at energy E_i, and $(\Delta E/E)_i^{rep}$ is the $10{\times}10^{-5}$ spread in fill energies at a given setting. The energy of an electron or positron bunch in a storage ring increases in an rf station and decreases in an arc. This implies that the center-of-mass collision energy is a function of position on the ring. Corrections must be applied for the variation of the cm energies at the LEP interaction regions (which vary by as much as 12 MeV). The uncertainties on these corrections contribute another 1 MeV to the energy-scale uncertainties of the experiments.

The Z mass is extracted from fits of a radiatively corrected Breit-Wigner lineshape to the cross sections measured at six, off-peak scan energies. More detail of this procedure is given in Sec. 4.2. The results are summarized in Table III. The energy scale uncertainty contributes 6 MeV to the overall error of each experiment. Uncertainties due to point-to-point luminosity errors and

Table III

Measurements of M_Z by the LEP Collaborations.[4]

Experiment	M_Z (GeV)	δM_Z (GeV)
ALEPH	91.187	0.009
DELPHI	91.186	0.009
L3	91.195	0.009
OPAL	91.181	0.009
Common Energy Scale Error		0.006
Combined Result	91.187	0.007

radiative corrections are much smaller than the 7 MeV statistical errors on each measurement.

3. Tree-Level Tests of the MSM

We consider next those electroweak tests that are sensitive primarily to the tree-level structure of the MSM Lagrangian or to the particle content of the theory. There are some electroweak measurements that clearly belong in this category (*e.g.*, the invisible width of the Z boson) but are more conveniently discussed in the next chapter on *loop-level tests*.

3.1 W/Z Cross Section Ratio

The CDF and D0 Collaborations have recently produced preliminary measurements[6,7] of the ratio of W and Z cross sections with their 1992–1993 data. They measure the ratio R_ℓ which is defined as follows:

$$R_\ell \equiv \frac{\sigma(p\bar{p} \to W \to \ell\nu)}{\sigma(p\bar{p} \to Z \to \ell\ell)} = \frac{\sigma(p\bar{p} \to W)}{\sigma(p\bar{p} \to Z)} \cdot \frac{\Gamma(W \to \ell\nu)}{\Gamma(Z \to \ell\ell)} \cdot \frac{\Gamma_Z}{\Gamma_W} = r_{W/Z} \cdot \frac{\Gamma(W \to \ell\nu)}{\Gamma(Z \to \ell\ell)} \cdot \frac{\Gamma_Z}{\Gamma_W}, \tag{5}$$

where $r_{W/Z}$ is the ratio of the total cross sections for W and Z production; and Γ_W and Γ_Z are the total widths of the two states, respectively. The measurement of the cross-section ratio has a number of advantages over measurements of the individual cross sections. Experimental uncertainties on the luminosity, efficiencies, and acceptances cancel completely or partially. The ratio of the total hadronic W and Z cross sections $r_{W/Z}$ is calculable to fairly high precision (1–2.5%) and does not depend strongly on Standard Model assumptions ($r_{W/Z}$ scales as $[M_W/M_Z]^{1.6}$). Finally, the quantity R_ℓ is sensitive to the particle content and relative coupling strengths of the W final states.

Table IV

The integrated luminosities ($\int dt\mathcal{L}$), event sample sizes (N_{evt}), backgrounds ($\mathcal{B}$), acceptances ($\mathcal{A}$), and efficiencies (ε) of the CDF and D0 lepton analyses.[6,7]

	CDF $W \to e\nu$	CDF $Z \to ee$	D0 $W \to e\nu$	D0 $Z \to ee$	D0 $W \to \mu\nu$	D0 $Z \to \mu\mu$
$\int dt\mathcal{L}$ (pb)	18.4	18.4	3.45	3.45	7.3	7.3
N_{evt}	10991	1053	2824	172	1576	93
$\mathcal{B}$ (%)	$10.9^{+.8}_{-.5}$	4.9±0.9	3.6±1.2	10.3±2.6	24±4	6±3
$\mathcal{A}$ (%)	33.8±0.6	37.2±0.6	46.9±3.6	42.0±3.5	22.1±1.2	26.6±2.3
ε (%)	74.9±1.3	73.1±1.5	68.0±5.0	46.0±6.7	37.2±7.0	22.5±5.3

The measurements of the two groups are summarized in Table IV. The CDF measurement is based on electron samples that incorporate most of their new data. The D0 Collaboration measurements are based on small samples of electron and muon final states. In order to minimize efficiency corrections, each group attempts to select W and Z events with similar criteria. All gauge boson candidates are required to contain a charged lepton that satisfies fairly strict selection criteria. The second lepton in Z events is then required to pass much less restrictive charged lepton identification criteria. The neutrino in W candidates is the (largely kinematic) requirement that missing transverse energy be present. The event totals for the six samples are listed in Table IV.

The event totals must be corrected for a number of backgrounds. The W samples can contain hadronic events which fake the lepton identification criteria, W decays into $\tau\nu$ final states where the τ decays leptonically, and Z decays to $\ell\ell$ and $\tau\tau$ where one final-state lepton is undetected. The Z samples can be contaminated by hadronic backgrounds, Z decays to $\tau\tau$ final states, electromagnetically produced lepton pairs, and cosmic ray muon events. The fractional backgrounds ($\mathcal{B}$) are listed with the selection criteria acceptances ($\mathcal{A}$) and efficiencies (ε) in Table IV. Note that the background for the D0 $W \to e\nu$ sample seems particularly small compared with the large efficiency-acceptance product for the event selection. This may be due to the excellent hermeticity of the D0 calorimeter in selecting events with missing transverse energy. It is also clear that the much older CDF Collaboration now has an excellent understanding of their acceptances and efficiencies.

The systematic uncertainties on the acceptance-efficiency products for W and Z events cancel in part. The resulting measurements of R_ℓ are:

$$R_\ell = \begin{cases} 10.64 \pm 0.36 \pm 0.27, & \text{CDF electrons} \\ 10.55 \pm 0.87 \pm 1.07, & \text{D0 electrons} \\ 10.0 \pm 1.1 \pm 2.4, & \text{D0 muons.} \end{cases}$$

The interpretation of these results requires a calculation of the ratio of total cross sections $r_{W/Z}$ at $\sqrt{s} = 1.8$ TeV. The two groups use slightly different values:

$$r_{W/Z} = \begin{cases} 3.23 \pm 0.03, & \text{CDF}\,[8] \\ 3.26 \pm 0.08, & \text{D0}.[9] \end{cases}$$

The ratio $R_\ell / r_{W/Z}$ is equal to the ratio of the W and Z leptonic branching ratios (see Eq. (5)). The Z leptonic branching ratios have been measured at the $4{\times}10^{-3}$ level by the LEP Collaborations (see Sec. 4.2.4). Using the calculated values $r_{W/Z}$ and LEP measurements of $\Gamma(Z \to \ell\ell)$ and Γ_Z, the CDF and D0 Collaborations quote the following results for the leptonic branching ratio of the W:

$$\frac{\Gamma(W \to \ell\nu)}{\Gamma_W} = \begin{cases} 0.1100 \pm 0.0036 \pm 0.0031, & \text{CDF (electrons)} \\ 0.108 \pm 0.013, & \text{D0 (electrons+muons).} \end{cases}$$

This way of quoting the results has the advantage that it minimizes MSM bias and is sensitive to the presence of new (unseen) W decays or to unexpected coupling differences among the final states. A second, more biased method is to use the measured value of Γ_Z and to assume that the ratio of leptonic widths $\Gamma(W \to \ell\nu)/\Gamma(Z \to \ell\ell)$ is correctly predicted by the MSM. Equation (5) can then be solved for the total width of the W,

$$\Gamma_W = \begin{cases} 2.033 \pm 0.069 \pm 0.057 \text{ GeV}, & \text{CDF} \\ 2.10 \pm 0.25 \text{ GeV}, & \text{D0}. \end{cases}$$

However, since we know that the leptonic branching ratio of the Z is quite close to the value predicted by the MSM, this approach implicitly fixes the leptonic width of the W to its MSM value. The resulting value of Γ_W contains no more information than does the leptonic branching ratio.

The measured values of the W leptonic branching ratio are used to extract limits on the top quark mass that are independent of assumptions about the top quark final states. The expected inverse branching ratio is plotted against the top mass in Fig. 2. The 95% upper limits from the preliminary CDF and D0 measurements are shown with the older, combined result[10] of the UA2 and CDF Collaborations. The resulting model-independent lower limits on the top quark mass are 42 GeV (D0) and 63 GeV (CDF).

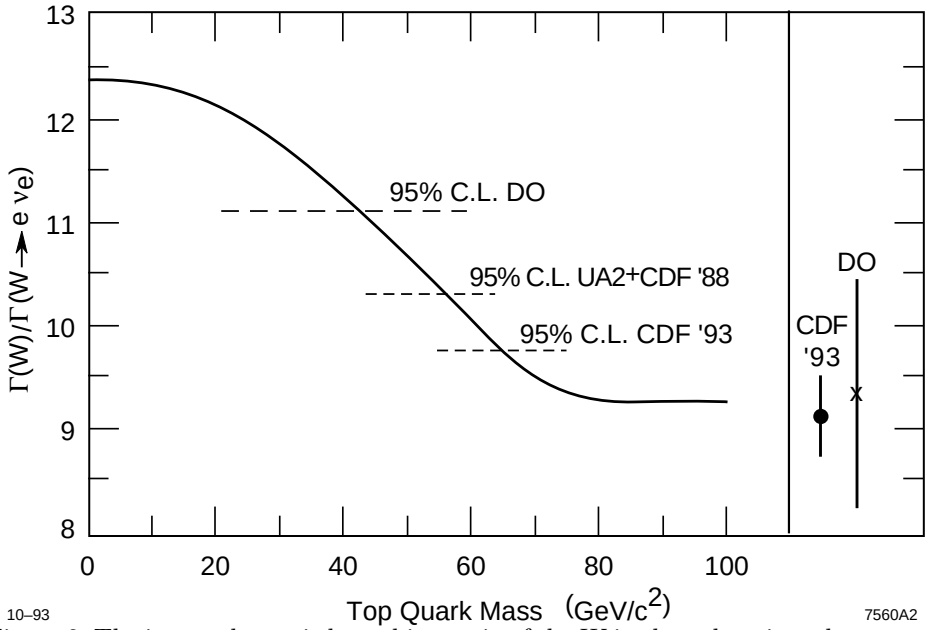

Figure 2. The inverse leptonic branching ratio of the W is plotted against the mass of the top quark. The 95% upper limits from the preliminary CDF and D0 measurements[6,7] are shown with the older, combined results[10] of the UA2 and CDF Collaborations. The resulting model-independent lower limits on the top quark mass are 42 GeV (D0) and 63 GeV(CDF).

3.2 The Search for Z'

The presence of a second neutral gauge boson would certainly affect the structure of the Electroweak Standard Model. Two groups have presented limits on the existence of such a state.

3.2.1 The CDF Search

The CDF Collaboration has searched[11] for the process $p\bar{p} \to Z' \to ee$ with a data sample corresponding to an exposure of 21 pb^{-1}. They search for events which satisfy their Z trigger and satisfy a set of selection criteria similar to that used to measure R_ℓ (one strictly selected central electron and one loosely selected electron in the entire instrumented acceptance). They observe 1244 ee candidates of mass larger than 44 GeV. The observed ee mass distribution is shown in Fig. 3. The largest observed mass is 320 GeV.

The net efficiency of the trigger and selection criteria is approximately 70%. The geometrical acceptance increases from 34.7% at the Z pole to 52% at a pair mass of 200 GeV and is roughly constant at larger masses. The limit on the product $\sigma(p\bar{p} \to Z') \cdot \mathrm{Br}(Z' \to e^+e^-)$ is extracted from a likelihood fit of the mass spectrum expected for the processes $p\bar{p} \to Z, Z' \to e^+e^-$ to the observed

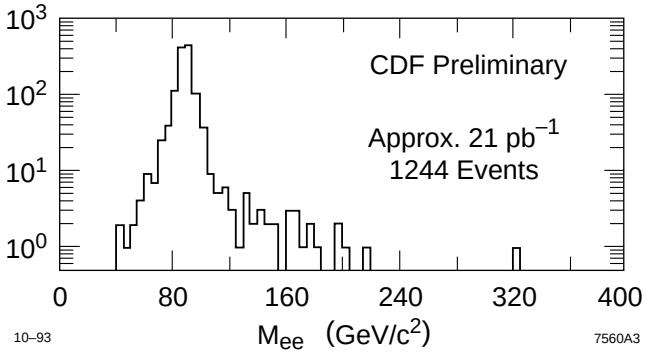

Figure 3. The mass distribution of 1244 ee events observed by the CDF Collaboration[11] in an exposure of 21 pb^{-1} in 1992–1993. The largest observed mass is 320 GeV.

mass spectrum. The limit is extracted for a series of Z' masses with the following assumptions:

1. The Z' is assumed to have the same couplings to $q\bar{q}$ and $\ell^+\ell^-$ as does the Z.
2. The top quark mass is assumed to be 150 GeV so that Z' can decay into $t\bar{t}$ if it is kinematically allowed.

Comparing the measured and expected lepton pair production cross sections, a 95% confidence lower limit on the Z' mass is extracted:

$$M_{Z'} < 495 \text{ GeV at } 95\% \text{ C.L.}$$

3.2.2 The L3 Search

The L3 Collaboration has searched[12] for the mixing of the Z with a larger-mass Z'. In this case, the state observed at 91 GeV is a mass eigenstate and is a mixture of the unmixed states Z^0 and $Z^{0\prime}$. The mixing is described by a simple rotation matrix,

$$\begin{pmatrix} Z \\ Z' \end{pmatrix} = \begin{pmatrix} \cos\theta_M & \sin\theta_M \\ -\sin\theta_M & \cos\theta_M \end{pmatrix} \begin{pmatrix} Z^0 \\ Z^{0\prime} \end{pmatrix}, \tag{6}$$

where θ_M is the mixing angle. The mixing angle is related to the mixed masses M_Z and $M_{Z'}$, and the light unmixed mass M_0 as follows:

$$\tan^2\theta_M = \frac{M_0^2 - M_Z^2}{M_{Z'}^2 - M_0^2}. \tag{7}$$

The unmixed mass participates in the Standard Model expression

$$M_0 = \frac{M_W}{\rho\cos\theta_W}, \tag{8}$$

where ρ is the usual electroweak parameter. The presence of mixing strongly affects the Z-fermion couplings and all of the Z-pole physical observables. The peak hadronic cross section and ratio of the leptonic and hadronic widths are sensitive to the strong coupling constant α_s but are insensitive to loop-level corrections. Together, they are particularly useful for Z' searches.[14] Recent searches include all of the measured Z-pole quantities.[15]

The L3 search is carried out by fitting a mixed-model to all of the measured Z lineshape parameters (see Sec. 4.4). The ρ parameter in Eq. (8) is assumed equal to 1. Several types of Z' bosons are considered:[13] Z'_χ, Z'_ψ, Z'_η, and Z'_{L-R}. The resulting limits are plotted in $M_{Z'}$-θ_M space in Fig. 4. The sensitivity of the search comes primarily from changes in the Z phenomenology caused by the mixing and not from Z' interference effects. The limits therefore extend to arbitrarily large values of $M_{Z'}$.

4. Loop-Level Tests of the MSM

The higher-order (loop-level) corrections to the various electroweak observables are functions of the unknown parameters of the MSM, the top quark mass (m_t), and the Higgs boson mass (m_H). This has the consequence that the measurement of a single electroweak observable does not (in general) test the model. The unknown parameters can usually be adjusted within the allowed regions to give agreement with the measurement. To actually perform meaningful tests, we therefore need measurements of several quantities that have distinct dependence on the unknown parameters. This approach has the additional benefit that observables with different dependence on m_t and m_H often have different sensitivity to extensions of the MSM. The measurement of complementary quantities will have considerable importance after m_t is measured, especially when deviations from the MSM are found. The classes of loop-level corrections to the tree-level electroweak Standard Model are illustrated in Fig. 5. The oblique or vacuum polarization corrections produce large effects due to the running of the electromagnetic coupling constant α_{em} and smaller (but measurable) effects due to heavy particles. The vertex corrections are expected to be small (but not negligible) and generally uninteresting. The corrections to the $Zb\bar{b}$ vertex are an exception. They are sensitive to m_t and to the presence of new physics. Finally, box diagrams produce very small corrections in the gauges that are used to perform the calculations and are generally ignored.

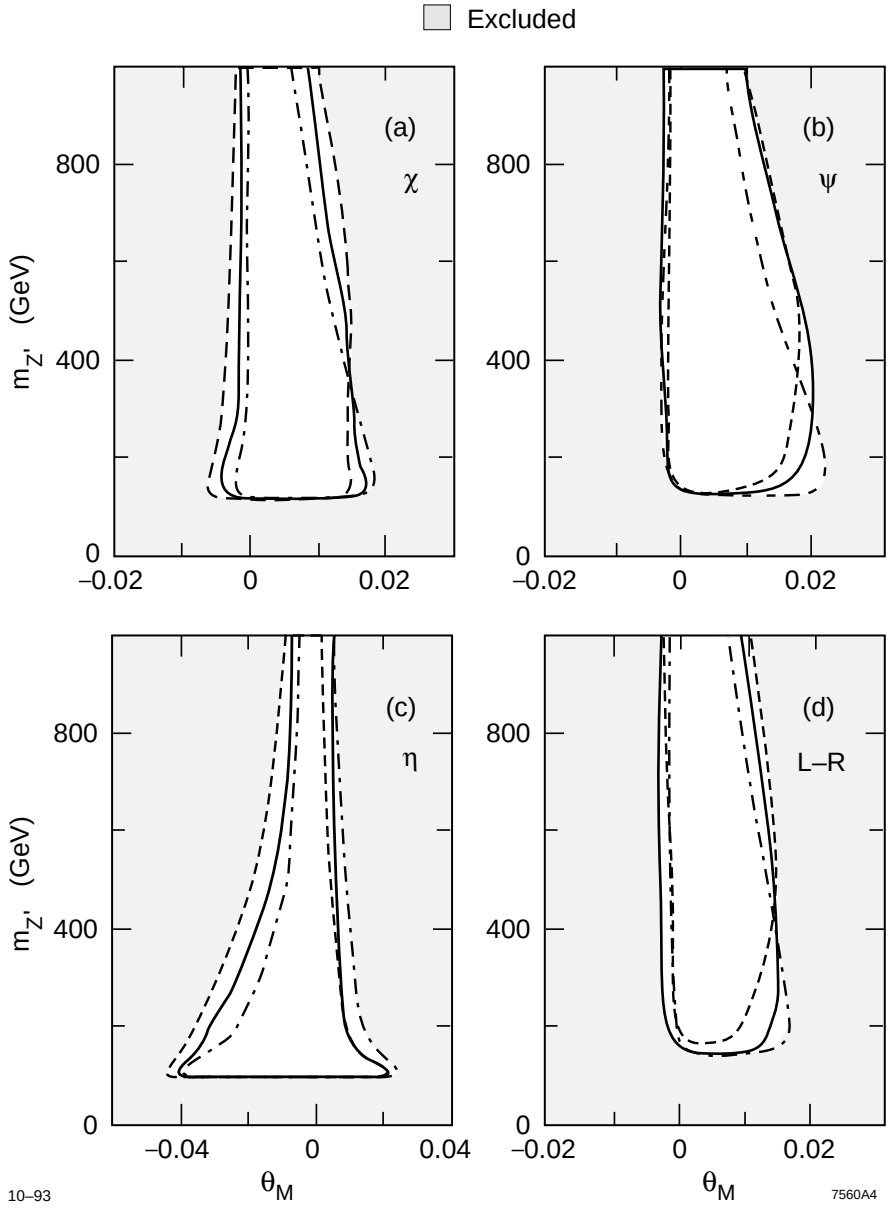

Figure 4. The 95% C.L. limits extracted by the L3 Collaboration[12] on the existence of a Z' mixed with the ordinary Z. The limits are shown in the space of mixing angle θ_M and mass $M_{Z'}$ for several Z' types.[13]

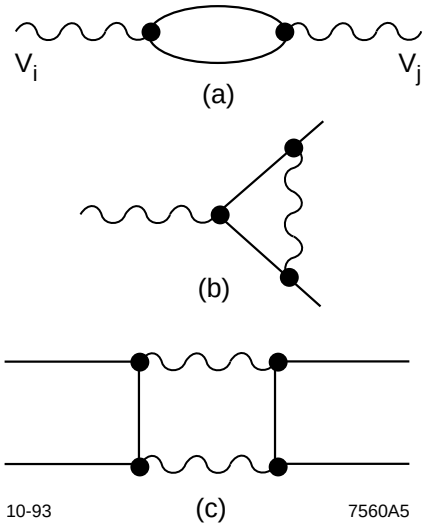

Figure 5. The classes of loop-level corrections to the MSM: a) oblique or vacuum polarization corrections, b) vertex corrections, and c) box diagrams.

There are two approaches loop-level testing of the MSM:

1. The MSM is simultaneously fit to all measured electroweak observables. The fit is used to estimate the unknown parameters, and the goodness of fit is an indicator of the validity of the model. This approach is esthetically clean and generally uninformative. Deviations from the MSM might affect only a small number of the measured observables. In this case, the goodness of fit would not be the most efficient indicator of the validity of the MSM.
2. A second approach is to attempt to characterize possible deviations in a *model-independent* way. Unfortunately, no truly model-independent approach has yet been proposed. Those that have been proposed make the not very radical assumptions that the MSM is correct at tree-level (the ρ parameter is unity at lowest order) and that the running of α_{em} due to light particle loops is correctly calculated. A number of three-parameter schemes have been suggested: the S,T,U scheme of Peskin and Takeuchi;[16] the S_Z,S_W,T scheme of Marciano and Rosner;[17] the h_{AZ},h_{AW},h_V scheme of Kennedy and Langacker;[18] and the ε_1,ε_2,ε_3 scheme of Altarelli, Barbieri, and Jadach.[19] These parameterizations differ somewhat in definition and concept (some include only oblique corrections, and others also incorporate vertex corrections). However, they are quite similar operationally, and to the extent that oblique corrections dominate, they are related by simple linear transformations.

For reasons of purely personal convenience, this talk is organized with the S,T,U scheme of Peskin and Takeuchi.

4.1 The S,T,U(V) Scheme

The S,T,U scheme is an approximation that is defined entirely in terms of the gauge boson self-energies $\Pi_{ij}(q^2)$ (see Fig. 5) where the indices i and j take the values 1,2,3,Q to indicate the gauge bosons W_1,W_2,W_3,A, respectively. To implement the scheme, these functions are approximated by the first two terms of a Taylor series,

$$\Pi_{ij}(q^2) = \Pi_{ij}(0) + q^2\Pi'_{ij}(q^2), \tag{9}$$

where the functions Π'_{ij} are the derivatives of Π_{ij} only at $q^2 = 0$.

The parameters S,T, and U are defined as follows:

$$\begin{aligned}
\alpha S &= 4e^2\left[\Pi'_{33}(0) - \Pi'_{3Q}(0)\right] \\
\alpha T &= \frac{e^2}{s_0^2 c_0^2 M_Z^2}\left[\Pi_{11}(0) - \Pi_{33}(0)\right] \\
\alpha U &= 4e^2\left[\Pi'_{11}(0) - \Pi'_{33}(0)\right],
\end{aligned} \tag{10}$$

where $\alpha = \alpha(M_Z^2)$ was defined in Eq. (1), and s_0 and c_0 are the sine and cosine functions of the angle θ_0,

$$\sin^2 2\theta_0 = \frac{4\pi\alpha(M_Z^2)}{\sqrt{2}G_F M_Z^2}.$$

The S parameter is weak isospin symmetric and characterizes the size of the sector that contributes to Π_{33}. It has a logarithmic dependence on m_t and m_H. The T parameter characterizes the degree of breaking of the custodial SU(2) symmetry that ensures the unity of the ρ parameter. It has an approximately quadratic dependence on m_t and a logarithmic dependence on m_H. In the MSM and many of its extensions, the U parameter is associated with somewhat smaller corrections than are S and T. It has a logarithmic dependence upon m_t and is independent of m_H. The effective Lagrangian for neutral current processes depends on S and T only. The charged current effective Lagrangian depends on S, T, and U. Since most of the electroweak observables that have been measured concern neutral current processes, and since U is associated with small effects in well-studied theories, it is customary to assume that U is zero.

The corrections that are associated with S and T typically alter the value of an electroweak observable by a few percent or less. Therefore, the S-T dependence of an observable is well-described by a simple linear expansion. The general scheme is to calculate the value of an observable O_i as accurately as is possible at

some reference value of m_t and m_H, $\bar{O}_i(m_t^{ref}, m_H^{ref})$. The value of the observable at other values of m_t and m_H is then given by the simple expansion,

$$O_i = \bar{O}_i(m_t^{ref}, m_H^{ref}) + a_i \left(S - S^{ref}\right) + b_i \left(T - T^{ref}\right), \tag{11}$$

where S^{ref} and T^{ref} are the values of S and T at m_t^{ref} and m_H^{ref} and where *the coefficients a_i and b_i are constants that are independent of the true values of S and T (m_t and m_h).*

The definitions of S and T in terms of gauge boson self-energies contain intrinsically arbitrary offsets. It is therefore convenient to redefine S and T to be $S - S^{ref}$ and $T - T^{ref}$, respectively. The conventional choice of reference point is (m_t^{ref}, m_H^{ref}) = (150 GeV, 1000 GeV).

A small problem arises when considering observables that depend on the strong coupling constant α_s. The current experimental uncertainty on α_s leads to non-negligible uncertainties on the predicted values $\bar{O}_i(m_t^{ref}, m_H^{ref})$. In the past, these uncertainties have been incorporated by increasing the experimental uncertainties on the affected observables. If the ensuing correlations are properly accounted, this technique does not sacrifice any sensitivity.

A more elegant approach is to properly recognize that the predicted values of the observables do depend on α_s and to include α_s as a free or constrained parameter. Fits to the data can then be used to estimate α_s. The uncertainty on S and T that is associated with the additional degree of freedom can be included by integrating over all values of α_s in the standard way. We therefore add to the S,T,U scheme, a fourth parameter V which is defined as the difference between α_s and a reference value, $V \equiv \alpha_s - \alpha_s^{ref}$. Equation (11) can now be expressed as

$$O_i = \bar{O}_i(m_t^{ref}, m_H^{ref}, \alpha_s^{ref}) + a_i \cdot S + b_i \cdot T + d_i \cdot V, \tag{12}$$

where d_i depends weakly on the reference value α_s. To minimize the V corrections, the reference value is chosen to be 0.123, which is indicated by various QCD measurements at the Z-pole.[20]

It is clear from Eqs. (11) and (12) that a measurement of an electroweak observable defines a linear confidence band in S-T space. It is also clear that observables with different S-T slopes $m_i^{ST} = -a_i/b_i$ provide different information about the electroweak Standard Model.

As an example, we can consider a set of three *old* electroweak measurements (in this case, old means that new results are not given in this talk): the ratio of the W and Z masses, M_W/M_Z;[21] the ratio of the neutral current and charged current cross sections in neutrino-nucleon scattering, R_ν;[22] and the effective weak charge extracted from measurements of atomic parity violation in the Cs atom,

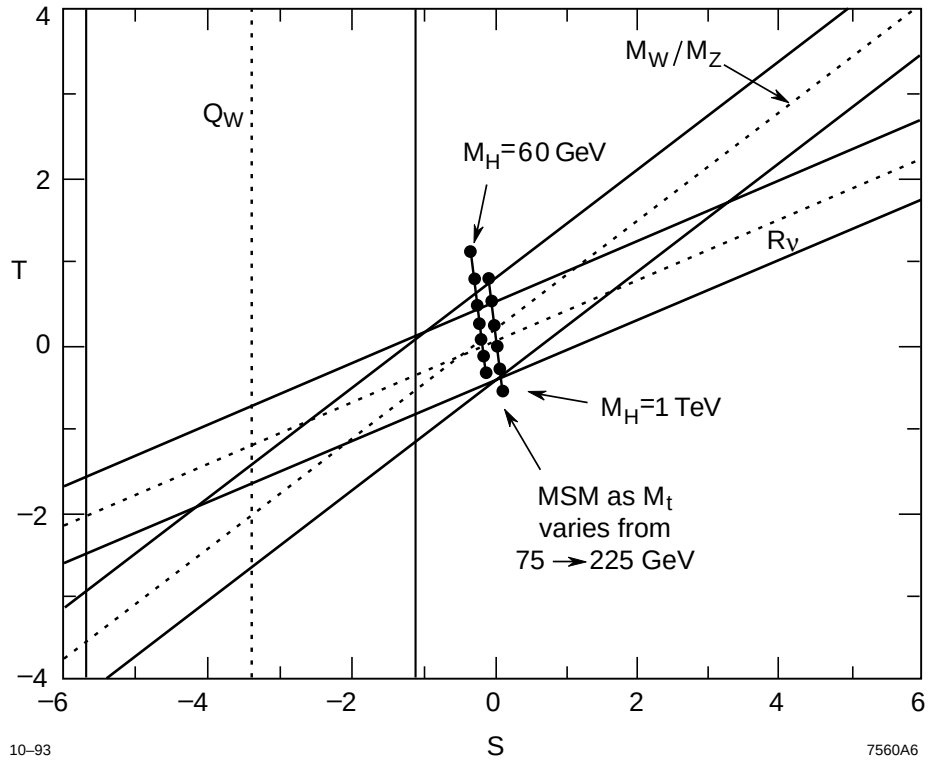

Figure 6. The 68% confidence regions in S-T space that are associated with the measurements listed in Table V. The vertical contours show the MSM predictions for m_H values of 60 GeV and 1000 GeV. The dots indicate various top quark masses between 75 GeV (bottom) and 225 GeV (top) in units of 25 GeV.

Table V

Existing measurements of several electroweak observables and their S,T,V parameters (see Eq. (12) for the parameter definitions). The parameters d_i are zero for these observables.

Obs.	Measured Value	$\bar{O}_i$ [24]	a_i [16]	b_i [16]	m^{ST}
M_W/M_Z	0.8789±0.0030 [21]	0.8791	-3.15×10^{-3}	4.86×10^{-3}	0.65
R_ν	0.312±0.003 [22]	0.3130	-2.32×10^{-3}	6.46×10^{-3}	0.36
Q_W(Cs)	−71.0±1.8 [23]	−73.4	-7.90×10^{-1}	-6.46×10^{-2}	−72

Q_W.[23] The current measurements of these quantities and their S-T slopes are listed in Table V. The corresponding 68% confidence regions in S-T space are shown in Fig. 6. The vertical contours show the MSM predictions for m_H values of 60 GeV and 1000 GeV. The dots indicate various top quark masses between 75 GeV (bottom) and 225 GeV (top) in units of 25 GeV.

Note that the interpretation of the quantity R_ν requires a knowledge of the quantity r which is defined as the ratio of antineutrino and neutrino charged current cross sections. We use the CDHS value[25] $r = 0.383$. It has recently become fashionable for neutrino experiments (CCFR) to quote their R_ν results solely in terms of the on-shell electroweak mixing parameter $\sin^2\theta_W \equiv 1 - M_W^2/M_Z^2$. This procedure requires the application of loop-level MSM electroweak corrections which, due to fortuitous cancellations,[26] have small m_t dependence. Unfortunately, the resulting value of $\sin^2\theta_W$ has an MSM bias. This is made clear by examining the S-T slopes of $\sin^2\theta_W$ (same as M_W/M_Z) and R_ν. They differ rather substantially (see Table V and Fig. 6). It is clear that these quantities are not equivalent. We urge the relevant parties to present their results in a less model-dependent way.

4.2 Z Lineshape Parameters

4.2.1 Definitions

The LEP Collaborations have measured a number of parameters that are associated with the cross sections for the processes $e^+e^- \to Z \to q\bar{q}$ and $e^+e^- \to Z \to \ell^+\ell^-$.

To excellent approximation, the hadronic cross section can be described by a radiatively corrected relativistic Breit-Wigner cross section,

$$\sigma_{had}(s_{lab}) = \int dx_1 dx_2 D_e(x_1) D_e(x_2) \frac{\sigma_0 \Gamma_Z^2 s^2/M_Z^2}{(s - M_Z^2)^2 + \Gamma_Z^2 s^2/M_Z^2}, \qquad (13)$$

where s_{lab} is square of the nominal center-of-mass energy, x_1 and x_2 are the momentum fractions carried by the electron and positron after radiating, $D_e(x)$ is the electron structure function, $s = s_{lab}x_1x_2$ is the cm energy after initial state radiation, M_Z is the Z mass, Γ_Z is the Z width, and σ_0 is the so-called peak cross section (actually not the maximum cross section). The peak cross section can be expressed in terms of the electronic and hadronic partial widths Γ_{ee} and Γ_{had} as follows:

$$\sigma_0 = \frac{12\pi}{M_Z^2} \cdot \frac{\Gamma_{ee}\Gamma_{had}}{\Gamma_Z^2}. \qquad (14)$$

The differential leptonic cross sections can be expressed as follows:

$$\frac{d\sigma_\ell}{d\cos\theta^*} = \sigma_{had}(s_{lab}) \cdot \frac{1}{R_\ell} \cdot \frac{3}{8}\left[1 + \cos^2\theta^* + \frac{8}{3}A_{FB}^\ell \cos\theta^*\right] F_\ell(\cos\theta^*), \qquad (15)$$

where θ^* is the angle of the outgoing lepton with respect to the incident electron direction, R_ℓ is the ratio of the leptonic and hadronic widths Γ_ℓ/Γ_{had}, $A_{FB}^\ell(s_{lab})$

is the empirical forward-backward asymmetry measured at s_{lab}, and F_ℓ is a correction factor to take the t channel process into account for final state electrons ($F_\mu = F_\tau = 1$ for all θ^*).

The measurements of $A_{FB}^\ell(s_{lab})$ must be fit to a Standard Model calculation to correct for Z-γ interference arising from off-pole energies, initial state radiation, and the imaginary part of the photon self-energy. The resulting *tree-level* asymmetries $A_{FB}^{\ell,0}$ are related to effective leptonic vector (g_V^ℓ) and axial-vector (g_A^ℓ) couplings of the Z as follows,

$$\begin{aligned} A_{FB}^{\ell,0} &= \frac{3}{4} \cdot \frac{2g_V^e g_A^e}{(g_V^e)^2 + (g_A^e)^2} \cdot \frac{2g_V^\ell g_A^\ell}{(g_V^\ell)^2 + (g_A^\ell)^2} \\ &= \frac{3}{4} \cdot A_e \cdot A_\ell, \end{aligned} \tag{16}$$

where the definitions of A_e and A_ℓ are obvious.

The leptonic partial widths can be expressed within this scheme as follows:

$$\Gamma_{\ell\ell} = \frac{G_F M_Z^3}{6\pi\sqrt{2}} \left[\left(g_V^\ell\right)^2 + \left(g_A^\ell\right)^2 \right] \cdot \left(1 + \frac{3\alpha}{4\pi}\right), \tag{17}$$

where the final state electromagnetic vertex correction is included explicitly. Equations (16) and (17) define the effective couplings g_V^ℓ and g_A^ℓ in terms of physical parameters. The couplings therefore contain the entire spectrum of electroweak radiative corrections.

It has become standard to define the effective electroweak mixing parameter $\sin^2\theta_W^{\rm eff}$ in terms of the ratio g_V^ℓ/g_A^ℓ,

$$\sin^2\theta_W^{\rm eff} \equiv 1 - 4g_V^\ell/g_A^\ell \simeq \left(\sin^2\theta_W^{\rm eff}\right)^{ref} + 0.0036 \cdot S - 0.0025 \cdot T, \tag{18}$$

where we have included the S-T trajectory relative to the reference value[24] $(\sin^2\theta_W^{\rm eff})^{ref} = 0.2336$. This S-T trajectory which has a slope of 1.4 describes most of the electroweak observables that are measured at the Z pole. As defined, the parameter $\sin^2\theta_W^{\rm eff}$ incorporates the electroweak vertex corrections that affect the $Z\ell\ell$ vertex. However to excellent approximation, it also describes the $Zq\bar{q}$ couplings

$$\sin^2\theta_W^{\rm eff} \simeq 1 - 4|Q_q|g_V^q/g_A^q, \tag{19}$$

where Q_q is a quark charge. The errors introduced by this approximation are at the level $\Delta\sin^2\theta_W^{\rm eff} \sim 1 - 2 \times 10^{-4}$ except for b quarks which have larger vertex corrections.

Table VI

A summary of the event samples used by the LEP Collaborations to measure various electroweak observables.[27] Event totals are given in thousands of events.

		ALEPH	DELPHI	L3	OPAL	LEP
$q\bar{q}$	'91-'92	451	365	423	454	1693
	'92	686	695	677	733	2791
	total	1137	1060	1100	1187	4484
$\ell^+\ell^-$	'91-'92	55	37	40	58	190
	'92	82	76	58	88	304
	total	137	113	98	146	494

4.2.2 The Measurements

The LEP Collaborations have recently produced a grand combination of all of their electroweak results from their 1990–1991 and 1992 runs.[27] This remarkable document is highly recommended to all workers in the field of precision electroweak testing.

The LEP results are based on total samples of 4×10^6 hadronic Z events and 0.5×10^6 leptonic events. The event samples of the individual experiments are summarized in Table VI.

Each group performs a nine-parameter simultaneous fit to its hadronic and leptonic data samples. The fit parameters are M_Z, Γ_Z, σ_0, R_e, R_μ, R_τ, $A_{FB}^{e,0}$, $A_{FB}^{\mu,0}$, and $A_{FB}^{\tau,0}$. The systematic uncertainties that affect this analysis are listed in Table VII. Note that the luminosity errors do not include the theoretical uncertainty on the small-angle Bhabha cross section. This uncertainty depends on the acceptance of each luminosity monitor. It is quoted as 0.25% for ALEPH and L3 and 0.3% for DELPHI and OPAL. The errors affecting the hadronic and leptonic cross section measurements are due to uncertainties on selection efficiencies and backgrounds. The systematic errors on the forward backward asymmetries are due to uncertainties on acceptances (probably very small), energy scale, and radiative corrections.

Table VII

A summary of the systematic errors that affect measurements of the Z lineshape and leptonic forward-backward asymmetries.[27] The common error due to the LEP energy scale uncertainty is not included.

	ALEPH		DELPHI		L3		OPAL	
	'91	'92 prel	'91	'92 prel	'91	'92 prel	'91	'92 prel
$\mathcal{L}^{(a)}$	0.45%	0.35%$^{(b)}$ 0.15%$^{(c)}$	0.5%	0.6%	0.5%	0.5%	0.60%	0.41%
σ_{had}	0.2%	0.17%	0.2%	0.28%	0.15%	0.14%	0.20%	0.20%
σ_e	0.4%	0.4%	0.5%	0.6%	0.4%	0.4%	0.45%	0.22%
σ_μ	0.5%	0.5%	0.5%	0.5%	0.5%	0.5%	0.25%	0.19%
σ_τ	0.6%	0.5%	0.75%	0.75%	0.7%	0.7%	0.76%	0.44%
A^e_{FB}	(d)	(d)	0.002	0.004	0.0045	0.002	0.003	0.002
A^μ_{FB}	(d)	(d)	0.003	0.002	0.003	0.003	0.003	0.001
A^τ_{FB}	(d)	(d)	0.002	0.004	0.006	0.003	0.003	0.002

$^{(a)}$Does not include the theoretical error on the small-angle Bhabha cross section. The theoretical error is acceptance dependent and is 0.25% for ALEPH and L3 and 0.3% for DELPHI and OPAL. $^{(b)}$Without the ALEPH silicon calorimeter. $^{(c)}$With the ALEPH silicon calorimeter. $^{(d)}$This error has not been accurately estimated since it is known to be smaller than the statistical error.

The results of the nine-parameter fits are listed in Table VIII. The combined LEP result accounts for common energy scale and luminosity uncertainties. We see that the measurements of R_ℓ and $A^{\ell,0}_{FB}$ are consistent with lepton universality. Assuming that lepton universality is valid, the data are then fit to a five-parameter hypothesis which depends on M_Z, Γ_Z, σ_0, R_ℓ, and $A^{\ell,0}_{FB}$. The results of this analysis are summarized in Table IX. Note that the individual errors within the five and nine parameter sets are correlated. The correlation matrices are reproduced in Appendix A.

4.2.3 Interpretation of the Lineshape Parameters

The hadronic width of the Z is affected by a 4% QCD vertex correction,

$$\Gamma_{had} = \Gamma^0_{had}\left(1 + \frac{\alpha_s}{\pi} + ...\right),$$

where Γ^0_{had} is the uncorrected width. This implies that the lineshape parameters Γ_Z, R_ℓ, and σ_0 depend on V (α_s). The S, T, and V dependence of these quantities

Table VIII

The results of nine-parameter fits to the hadronic and leptonic cross sections measured by the four LEP experiments.[27] The LEP totals include common energy scale and luminosity errors.

Param	ALEPH	DELPHI	L3	OPAL	LEP
M_Z (GeV)	91.187(9)	91.187(9)	91.195(9)	91.182(9)	91.187(7)
Γ_Z (GeV)	2.501(11)	2.482(12)	2.493(10)	2.483(12)	2.489(7)
σ_0 (nb)	41.61(16)	41.02(27)	41.33(26)	41.71(23)	41.56(14)
R_e	20.58(15)	20.70(18)	20.90(16)	20.83(16)	20.743(80)
R_μ	20.82(15)	20.48(15)	21.02(16)	20.78(11)	20.764(69)
R_τ	20.62(17)	20.88(20)	20.78(20)	21.01(15)	20.832(88)
$A_{FB}^{e,0}$	0.0185(59)	0.0237(92)	0.0135(78)	0.0062(80)	0.0153(38)
$A_{FB}^{\mu,0}$	0.0147(47)	0.0143(50)	0.0167(64)	0.0099(42)	0.0132(26)
$A_{FB}^{\tau,0}$	0.0182(53)	0.0213(68)	0.0257(89)	0.0205(52)	0.0204(32)
χ^2/dof					27.1/27

Table IX

The results of five-parameter fits to the hadronic and leptonic cross sections measured by the four LEP experiments.[27] The LEP totals include common energy scale and luminosity errors.

Param	ALEPH	DELPHI	L3	OPAL	LEP
M_Z (GeV)	91.187(9)	91.187(9)	91.195(9)	91.181(9)	91.187(7)
Γ_Z (GeV)	2.501(11)	2.482(12)	2.493(10)	2.482(12)	2.489(7)
σ_0 (nb)	41.61(16)	41.02(27)	41.33(26)	41.70(23)	41.56(14)
R_ℓ	20.68(10)	20.65(11)	20.92(11)	20.835(86)	20.763(49)
$A_{FB}^{\ell,0}$	0.0168(32)	0.0179(38)	0.0178(44)	0.0128(30)	0.0158(18)
χ^2/dof					30.8/31

are listed in Table X. Note that R_ℓ and σ_0 are simple functions of $\sin^2\theta_W^{\rm eff}$ and have the characteristic S-T slope of 1.4 (all wavefunction renormalization terms cancel). The total width is unique among the directly measured Z parameters in that its S-T trajectory differs from $m^{ST} = 1.4$.

The 68% confidence regions in S-T space that are associated with the V-dependent lineshape parameters are plotted in Fig. 7. For simplicity, the contours are plotted at $V = 0$. Note that σ_0 is particularly insensitive to S and T. It therefore determines V more or less independently of S and T. The vertical contours show the same MSM predictions that are plotted in Fig. 6.

Table X

The S, T, and V dependence of the lineshape parameters (see Eq. (12) for the definitions).

Observable	$\bar{O}_i$ [24]	a_i [16]	b_i [16]	d_i	m^{ST}
Γ_Z (GeV)	2.485	-9.58×10^{-3}	2.62×10^{-2}	5.87×10^{-1}	0.37
σ_0 (nb)	41.447	2.19×10^{-2}	-1.55×10^{-2}	-5.58	1.4
R_ℓ	20.753	-5.99×10^{-2}	4.24×10^{-2}	7.01	1.4

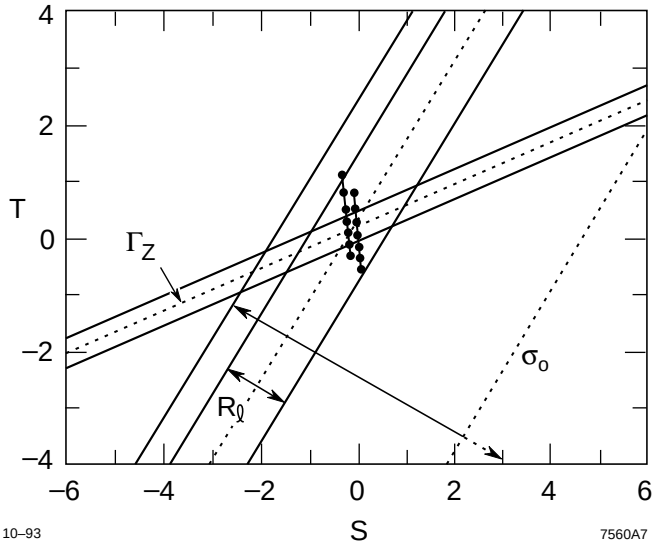

Figure 7. The 68% confidence regions in S-T space that are associated with the V-dependent lineshape parameters Γ_Z, R_ℓ, and σ_0. The contours are plotted at $V = 0$. The vertical contours show the MSM predictions for m_H values of 60 GeV and 1000 GeV. The dots indicate various top quark masses between 75 GeV (bottom) and 225 GeV (top) in units of 25 GeV.

4.2.4 Derived Lineshape Parameters

A number of quantities can be derived from the five- and-nine parameter sets of measured quantities. These derived parameters obviously do not contain any additional information regarding the validity of the MSM but are useful for other purposes. Using the definitions of R_ℓ and σ_0 (see Eq. (14)), it is straightforward to determine the hadronic and leptonic widths, Γ_{had} and $\Gamma_{\ell\ell}$, from the measured parameters M_Z, Γ_Z, R_ℓ, and σ_0. The invisible width $\Gamma_{inv} \equiv \Gamma_Z - \Gamma_{had} - 3\Gamma_{\ell\ell}$ follows in straightforward fashion. The vector and axial vector couplings, g_V^ℓ and g_A^ℓ, can be determined from the parameters $A_{FB}^{\ell,0}$ and $\Gamma_{\ell\ell}$. Finally, it is straightforward to determine the parameter $\sin^2\theta_W^{\rm eff}$ from the forward-backward asymmetries $A_{FB}^{\ell,0}$.

Table XI

Parameters that are derived from the measured lineshape parameters of the LEP Collaborations.[27]

Without Lepton Universality	
Γ_{ee} (MeV)	83.86±0.30
$\Gamma_{\mu\mu}$ (MeV)	83.78±0.40
$\Gamma_{\tau\tau}$ (MeV)	83.50±0.45
With Lepton Universality	
$\Gamma_{\ell\ell}$ (MeV)	83.82±0.27
Γ_{had} (MeV)	1740.3±5.9
Γ_{inv} (MeV)	497.6±4.3
$(g_V^\ell)^2$	0.00134±0.00015
$(g_A^\ell)^2$	0.25088±0.00083
$\sin^2\theta_W^{\rm eff}$	0.2318±0.0010

The derived lineshape parameters are listed in Table XI. Note that the full error matrices have been used to account for correlations among the measured parameters.

The derived value for the ratio of the invisible and leptonic widths is $\Gamma_{inv}/\Gamma_{\ell\ell} = 5.936 \pm 0.054$. This ratio is converted into the number of light neutrinos N_ν by dividing by the MSM value for the ratio of neutrino and leptonic widths, $\Gamma_{\nu\nu}/\Gamma_{\ell\ell} = 1.993 \pm 0.003$. The result is in excellent agreement with the three-light-neutrino structure of the MSM,

$$N_\nu = 2.980 \pm 0.027.$$

4.3 Final-State Polarization of the τ

The process $e^+e^- \to Z \to f\bar{f}$ produces polarized final state fermions. Defining the polarization in terms of a left-handed basis, the final state polarization is expected to have the following dependence on couplings and the fermion direction:

$$\mathcal{P}_f = \frac{A_f(1+\cos^2\theta^*) + 2A_e\cos\theta^*}{1+\cos^2\theta^* + 2A_eA_f\cos\theta^*}, \tag{20}$$

where A_e and A_f are defined in Eq. (16). When averaged over all angles, the average final-state fermion polarization $\bar{\mathcal{P}}_f$ is simply A_f.

The τ is the only short-lived final-state fermion that is well-enough understood to serve as a polarimeter. In general, the decay of a polarized τ^- can

Table XII

Typical characteristics of $\mathcal{P}_\tau$ measurements with various final states. The analyzing power a_p is defined as the product $\delta\mathcal{P}_\tau \cdot \sqrt{N_{dec}}$.

Final State	$e\nu\bar{\nu}$	$\mu\nu\bar{\nu}$	$\pi\nu$	$\rho\nu$	$a_1\nu$
Branching Ratio (%)	18	18	12	24	8
Acceptance	0.4	0.7	0.6	0.5	0.5
Analyzing Power a_p	5	5	1.8	2.3	3.1
Relative Precision	2.7	2.1	1.0	1.0	2.2

be described by an N-dimensional decay distribution that has a linear dependence upon $\mathcal{P}_\tau$,

$$\frac{1}{\Gamma}\frac{d^N\Gamma}{dx^N} = A(x_1, ..., x_N) + \mathcal{P}_\tau B(x_1, ..., x_N), \tag{21}$$

where A and B are calculable functions. In practice, two-body hadronic final states ($\pi\nu$, $\rho\nu$, and $a_1\nu$) have the largest analyzing powers, and the three-body leptonic final states are the second most efficient. For π and ℓ final states, one kinematic variable describes the visible final state ($N = 1$). The ρ and a_1 final states are described by three and six kinematic variables, respectively.

The final-state polarization is measured by isolating a sample of particular τ final states and fitting the appropriate version of Eq. (21) to the measured kinematic distributions. The features of typical $\mathcal{P}_\tau$ measurements with the various final states are listed in Table XII. The analyzing power a_p characterizes the statistical precision $\delta\mathcal{P}_\tau$ that is obtainable with a sample of N_{dec} decays, $\delta\mathcal{P}_\tau = a_p/\sqrt{N_{dec}}$. The $\pi\nu$ final state has the best analyzing power but is comparable in overall precision with the more copious $\rho\nu$ final state.

Measurements of $\mathcal{P}_\tau$ are sensitive to uncertainties in the detector acceptances, backgrounds, interchannel cross talk, and energy scales. The $a_1\nu$ final state is sufficiently complex that the hadronic decay chain must be modelled which leads to a systematic uncertainty. The most precise $\mathcal{P}_\tau$ measurements have been performed by the ALEPH Collaboration.[28] The systematic uncertainties that are associated with their analyses are summarized in Table XIII.

Two of the LEP Collaborations (ALEPH and OPAL) have measured $\mathcal{P}_\tau$ as a function of θ^* and have used Eq. (20) to extract A_e in addition to A_τ. Small corrections ($\sim$0.002–0.003) must be applied to A_τ and A_e to account for Z-γ interference arising from the usual sources. The results are listed in Table XIV.

Table XIII

The systematic uncertainties that affect the ALEPH τ polarization measurements.[28]

Uncertainty	$e\nu\bar{\nu}$	$\mu\nu\bar{\nu}$	$\pi\nu$	$\rho\nu$	$a_1\nu$
Acceptance	0.011	0.012	0.016	0.024	0.014
τ Background	0.016	0.012	0.010	0.007	0.020
Non-τ Background	0.012	0.008	0.002	0.003	—
Energy Calibration	0.032	0.014	0.001	0.012	0.001
Model Dependence	—	—	—	—	0.012
Monte Carlo Stat.	0.021	0.017	0.008	0.010	0.020
Total Syst. Error	0.045	0.029	0.018	0.030	0.034

Table XIV

The parameters A_τ and A_e that are extracted from τ polarization by the LEP Collaborations.[27]

Experiment	A_τ	A_e
ALEPH ('90+'91)	0.143±0.023	0.120±0.026
DELPHI ('90+'91+'92)	0.151±0.029	—
L3 ('90+'91+'92)	0.133±0.024	—
OPAL ('90+'91)	0.117±0.046	0.231±0.083
LEP Average	0.139±0.014	0.130±0.025
χ^2/dof	0.5/3	1.6/1

4.4 Lepton Universality

For each lepton flavor, the measured forward-backward asymmetry and partial width determine the couplings g_V and g_A. The values of A_τ and A_e that are extracted from the τ polarization measurements are used to improve the determinations of the τ and electron couplings. The 1σ (39%) confidence region in the g_V-g_A space of each flavor is shown in Fig. 8. Note that they are consistent with lepton universality. If lepton universality is assumed, the data determine the solid ellipse.

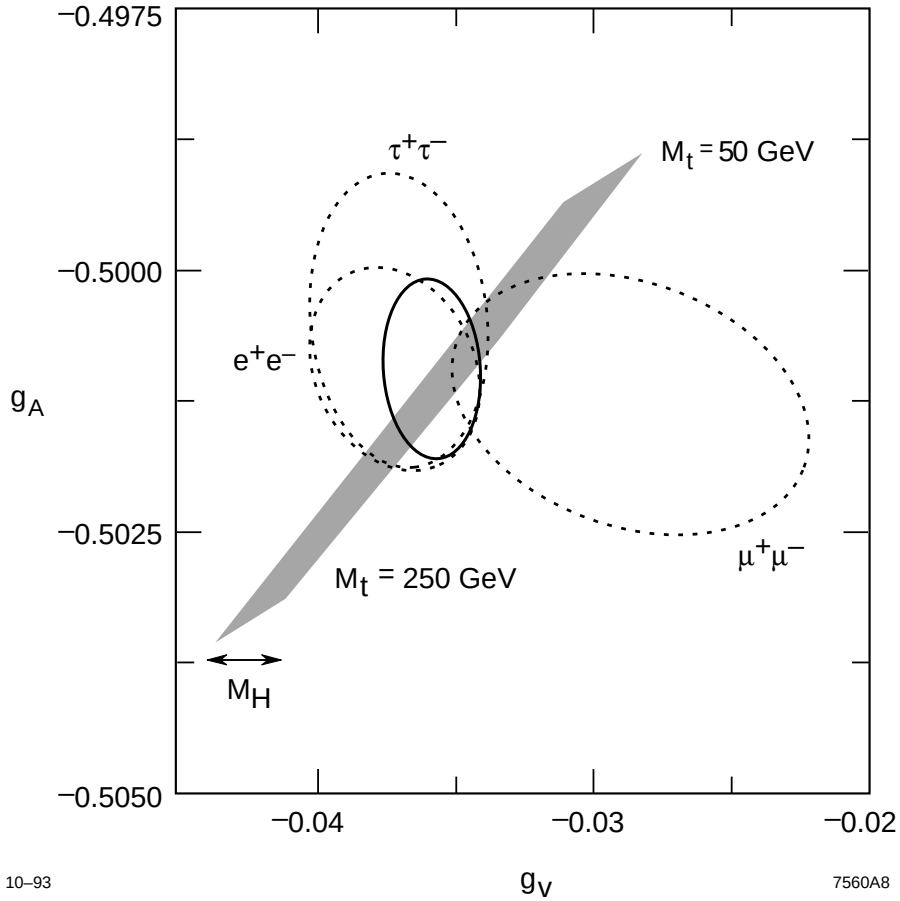

Figure 8. The 1σ (39%) confidence regions in g_V-g_A space that are extracted from measurements of $A_{FB}^{\ell,0}$, $\Gamma_{\ell\ell}$, A_τ, and A_e for the three lepton flavors.[27] The shaded region shows the MSM expectation.

The best estimates of g_V^ℓ and g_A^ℓ are listed in Table XV. The vector and axial vector coupling ratios are as follows:

$$g_V^\mu/g_V^e = 0.77 \pm 0.21 \qquad g_A^\mu/g_A^e = 1.0006 \pm 0.0026$$
$$g_V^\tau/g_V^e = 1.00 \pm 0.13 \qquad g_A^\tau/g_A^e = 0.9990 \pm 0.0029.$$

The axial vector couplings are consistent with universality at the 0.3% level. The much smaller vector couplings are consistent with lepton universality at the 10–20% level.

Table XV

The vector and axial vector leptonic couplings extracted from measurements of $A_{FB}^{\ell,0}$, $\Gamma_{\ell\ell}$, A_τ, and A_e by the LEP Collaborations.[27]

Without Lepton Universality	
g_V^e	-0.0373±0.0031
g_V^μ	-0.0288±0.0064
g_V^τ	-0.0372±0.0032
g_A^e	-0.50096±0.00093
g_A^μ	-0.5013±0.0012
g_A^τ	-0.5005±0.0014
With Lepton Universality	
g_V^ℓ	-0.0359±0.0018
g_A^τ	-0.50093±0.00082

4.5 Quark Forward-Backward Asymmetries

At the Z pole, the quark forward-backward asymmetries are also sensitive measures of $\sin^2\theta_W^{\rm eff}$. At $\sin^2\theta_W^{\rm eff} \simeq 0.232$, derivatives of the u- and d-quark asymmetries with respect to $\sin^2\theta_W^{\rm eff}$ are quite large,

$$\frac{dA_{FB}^u}{d\sin^2\theta_W^{\rm eff}} \simeq -4.3 \quad \text{and} \quad \frac{dA_{FB}^d}{d\sin^2\theta_W^{\rm eff}} \simeq -5.6.$$

To measure these asymmetries, it is necessary to identify the final state quark or mixture of final state quarks and to identify the quark (as opposed to antiquark) direction.

4.5.1 Average Quark Asymmetries

The simplest technique is to sum over all final-state quark flavors. The q direction must be determined on a statistical basis from total charges of the jets. The determination the q direction is complicated by the fact that the negatively charged hemisphere is the forward direction for d-type quarks and the backward hemisphere for u-type quarks. The charge determination is based on a quantity known as the momentum weighted jet charge which is calculated from the charged tracks in each event,

$$Q \equiv \frac{\sum q_i {\rm sgn}(\vec{p}_i \cdot \hat{T}) |\vec{p}_i \cdot \hat{T}|^\kappa}{\sum |\vec{p}_i \cdot \hat{T}|^\kappa}, \tag{22}$$

where q_i is the charge sign of the i^{th} track, $\vec{p}_i$ is the momentum of the i^{th} track, κ is a weighting exponent, and $\hat{T}$ is the direction of the thrust axis.

The quantity Q is used in two different ways. In the first, the z component of the thrust axis is taken to be positive (in the incident electron direction). In this case, the average value of Q is the so-called forward-backward jet charge Q_{FB}. The expected value of this quantity is given by the following expression:

$$Q_{FB} = \frac{1}{\Gamma_{had}} \sum_f \alpha_f \cdot 2Q_f A^f_{FB} \cdot \Gamma_{ff}, \tag{23}$$

where f labels the final state quarks, α_f is an analysis and detector dependent analyzing power, and Q_f is the quark charge. It is clear from Eq. (23) that the u-type quarks with (Q_u, A^u_{FB}, Γ_{uu}) of (2/3, $\sim$0.067, 297 MeV) tend to cancel the effects of the d-type quarks which are described by the parameters ($-1/3$, $\sim$0.095, 383 MeV). The resulting value of Q_{FB} is very small ($\simeq -0.006$)

The second way to use the momentum-weighted jet charge is to assign the q direction as the thrust direction such that Q is negative. The data can then be fit to the usual angular distribution,

$$\frac{dN}{d\cos\theta^*} = \frac{3}{8}\left[1 + cos^2\theta^* + \frac{8}{3}A^h_{FB}\cos\theta^*\right], \tag{24}$$

where A^h_{FB} is now an average quark asymmetry. The expected value of A^h_{FB} is given by the following expression:

$$A^h_{FB} = \frac{1}{\Gamma_{had}} \sum_f \alpha_f \cdot \frac{-Q_f}{|Q_f|} A^f_{FB} \cdot \Gamma_{ff}. \tag{25}$$

This quantity weights each quark component with unit weight (instead of the quark charge). The d-type quarks dominate the average which results in a larger asymmetry ($\sim$0.04).

The interpretation of either Q_{FB} or A^h_{FB} requires a knowledge of the analyzing powers. These must be derived from detailed simulations of the fragmentation process and detector response. However if one has a flavor-tagged sample, it is possible to determine α_f directly from the data by using the correlation between the Q measured in opposite thrust hemispheres.

The ALEPH and DELPHI Collaborations have performed measurements of Q_{FB}, and the OPAL Collaboration has performed a measurement of A^h_{FB}. Since the measured quantities depend on analyzing powers which are particular to the individual measurements, the results are quoted in terms of $\sin^2\theta^{\rm eff}_W$. The results are listed in Table XVI. The JETSET fragmentation model[29] is used by the experiments to calculate their analyzing powers. The results are most sensitive to the JETSET s/u parameter which describes strange quark production

Table XVI

The values of $\sin^2\theta_W^{\rm eff}$ determined from measurements of the average quark forward-backward asymmetries by the LEP Collaborations.[27]

Experiment	Measurement	s/u	$\sin^2\theta_W^{\rm eff}$
ALEPH (89-92)	Q_{FB}	0.315±0.045	0.2317±0.0013±0.0011
DELPHI (90-91)	Q_{FB}	0.315±0.045	0.2345±0.0030±0.0027
OPAL (90-91)	A_{FB}^h	0.285±0.050	0.2321±0.0017±0.0028
Average			0.2320±0.0011±0.0011

from string-breaking. The allowed ranges for this parameter are also listed in Table XVI. The systematic error on the ALEPH measurement has improved markedly this year.[30] This Q_{FB} measurement is now as precise as the individual three-flavor measurements of $A_{FB}^{\ell,0}$.

4.5.2 Heavy Quark Forward-Backward Asymmetries

The dilution of the measured asymmetries can be avoided by the use of flavor tagging. Accurate flavor tagging is possible only with b and c quarks. Three techniques are currently used to do this:

1. The traditional technique is to use large p-p_t leptons to tag the flavor and sign of the final-state jets. The mixing-diluted b-quark asymmetry $\bar{A}_{FB}^b$ and the c-quark asymmetry A_{FB}^c are extracted from a fit to the observed p-p_t spectrum. The model used in the fitting procedure must contain a number of lepton sources:
   (a) $b \to \ell^-$ which occurs with asymmetry $\bar{A}_{FB}^b$;
   (b) $b \to \tau^- \to \ell^-$ which occurs with asymmetry $\bar{A}_{FB}^b$;
   (c) $b \to c \to \ell^+$ which occurs with asymmetry $-\bar{A}_{FB}^b$;
   (d) $b \to \bar{c} \to \ell^-$ which occurs with asymmetry $\bar{A}_{FB}^b$;
   (e) $b \to J/\psi \to \ell^-$ which occurs with zero asymmetry; and
   (f) $c \to \ell^+$ which occurs with asymmetry $-A_{FB}^c$.
2. The advent of high-precision vertex detectors has lead to the use of lifetime tagging techniques to isolate fairly pure samples of b final states. The b-$\bar{b}$ separation is then achieved with the momentum-weighted jet charge technique. The determination of the jet charge analyzing power is substantially more reliable in this case for two reasons. The first is that the b-quark fragmentation function is peaked at large momentum fraction. The large momentum tracks in the event are mostly from the b-hadron decay chains which are well-measured and modelled. The second reason is

that with a relatively pure b sample, the analyzing power can be directly extracted from the data by using the correlation between the jet charge measured in opposite thrust hemispheres.

3. Prompt c quarks and c quarks from b decays can fragment into D^{*+} mesons. These decay into the following easily recognized and charge signed states:

$$D^{*\pm} \to \pi^{\pm} \begin{pmatrix} D^0 \\ \bar{D}^0 \end{pmatrix} \to \pi^{\pm}(K^{\mp}\pi^{\pm}),\ \pi^{\pm}(K^{\mp}\pi^{\pm}\pi^0),\ \text{and}\ \pi^{\pm}(K^{\mp}\pi^{\pm}\pi^{\mp}\pi^{\pm}).$$

The b-quark asymmetries are diluted by B^0-$\bar{B}^0$ mixing. The dilution is described by the following expression:

$$\bar{A}^b_{FB} = (1 - 2\chi_M) A^b_{FB}, \tag{26}$$

where χ_M is the well-known mixing parameter that is measured from the ratio of like-sign and opposite-sign dilepton events. The LEP Collaborations use the following value to correct their A^b_{FB} measurements,

$$\chi_M = 0.115 \pm 0.009 \pm 0.006.$$

The results of six measurements of A^b_{FB} and six measurements of A^c_{FB} performed by the LEP Collaborations are summarized in Table XVII. The common systematic errors are itemized in the central regions of the table.

The asymmetries listed in Table XVII must be corrected for final-state gluon radiation and electroweak interference arising from off-peak energies and initial-state radiation. The corrected values are

$$A^{b,0}_{FB} = 0.099 \pm 0.006 \quad \text{and} \quad A^{c,0}_{FB} = 0.075 \pm 0.015.$$

The interpretation of these numbers is discussed in Sec. 4.7.

4.6 Left-Right Asymmetry

In 1992, the SLD Collaboration performed the first measurement of the left-right Z cross section asymmetry A_{LR}.[31] This quantity is defined in terms of the cross sections for producing Z bosons with left- and right-handed electron beams, σ_L and σ_R, respectively. Assuming that the beam polarization is $\mathcal{P}_e$, the measured asymmetry has a particularly simple form,

$$A^{raw}_{LR} \equiv \frac{\sigma_L - \sigma_R}{\sigma_L + \sigma_R} = \mathcal{P}_e \cdot A_{LR} = \mathcal{P}_e \cdot A_e, \tag{27}$$

where $A_{LR} = A_e$ directly determines $\sin^2\theta^{\text{eff}}_W$. Note that A_{LR} has the following properties: it is a sensitive function of $\sin^2\theta^{\text{eff}}_W$, it is large (0.1–0.2), and it does not depend on the couplings of the Z to its final states.

Table XVII

A summary of the b-quark and c-quark forward-backward asymmetry measurements that have been performed by the LEP Collaborations.[27]

	ALEPH ℓ, high p_t 90–92	DELPHI μ, high p_t 91–92	L3 ℓ 90–92	OPAL ℓ 90–91	ALEPH vertex 92	DELPHI vertex 91–92	LEP avg.
A^b_{FB} (%)	8.1	10.2	9.1	9.1	10.9	11.6	9.4
Stat. error	±1.0	±1.6	±1.0	±1.8	±1.2	±1.9	±0.5
Uncorr. Sys.	±0.1	±0.9	±0.5	±0.4	±0.5	±1.7	±0.2
SL Model	±0.12	(b)	(b)	±0.30	(d)	(d)	
SL BR	±0.09	±0.46	±0.18	±0.25	(d)	(d)	
Fragment.	±0.12	±0.46	±0.08	±0.05	±0.10	±0.80	
Γ_{bb}/Γ_{cc}	±0.08	(b)	±0.04	±0.45	±0.11	±0.50	
Mixing	±0.23	±0.30	±0.26	±0.26	±0.13	±0.30	
A^c_{FB}	(c)	±0.46	(a)	(a)	(c)	(e)	
Total Corr.	±0.3	±0.8	±0.3	±0.6	±0.2	±1.0	±0.3
$\sqrt{s}$	91.27	91.27	91.27	91.23	91.28	91.27	91.27
χ^2/dof							3.8/5
	ALEPH ℓ 90–91	L3 ℓ 90–92	OPAL ℓ 90–91	ALEPH D^* 90–91	DELPHI D^* 90–91	OPAL D^* 91–92	LEP avg.
A^c_{FB} (%)	9.9	6.0	1.4	6.8	10.7	5.2	6.6
Stat. error	±2.0	±2.2	±3.0	±4.2	±7.5	±2.8	±1.2
Uncorr. Sys.	±1.5	±2.2	±1.7	±0.7	±1.0	±0.9	±0.7
SL Model	±0.76	(b)	±0.62	(d)	(d)	(d)	
SL BR	±0.51	±1.31	±0.66	(d)	(d)	(d)	
Fragment.	(a)	±0.45	±0.21	±0.18	±0.13[f]	±0.12	
Γ_{bb}/Γ_{cc}	(a)	±0.22	±0.60	(a)	(f)	(a)	
Mixing,A^b_{FB}	(d, a)	(d, a)	(d, a)	±0.54	±0.86[f]	±0.80	
D^* BR	(d)	(d)	(d)	±0.18	±0.13[f]	±0.12	
Total Corr.	±0.9	±1.4	±1.1	±0.6	±0.9	±0.8	±0.7
$\sqrt{s}$	91.23	91.27	91.23	91.23	91.23	91.27	91.25
χ^2/dof							4.5/5

[a]Fitted simultaneously and included in the statistical or uncorrelated error. [b]Treated together with the SL BR error. [c]Standard Model relationship of A^b_{FB} and A^c_{FB} is assumed. [d]Not applicable. [e]Negligible. [e]Breakdown of systematic error inferred from other D^* tag measurements.

Table XVIII

The properties of several Z pole asymmetry measurements. It is assumed that $x \equiv \sin^2\theta_W^{\rm eff} = 0.232$.

Property	A_{LR}^{raw}	A_{FB}^{ℓ}	A_{FB}^{b}	$\bar{\mathcal{P}}_\tau$
Asymmetry Size	$0.14\mathcal{P}_e$	0.016	0.099	0.14
Fraction of Visible Z Decays	96%	$3 \times 4\%$	19%	4%
Efficiency(ε) $\times$ Acceptance($\mathcal{A}$)	90%	70-80%	$\sim$10%	$\sim 30\%/\tau$
Sensitivity to $\sin^2\theta_W^{\rm eff}$ $(\partial A/\partial x)$	$7.9\mathcal{P}_e$	1.7	5.6	7.9
$\mathcal{P}_e$ Correction	yes	no	no	no
$\varepsilon \times \mathcal{A}$ Correction	no	yes	yes	yes
Background Correction	no	no	yes	yes
$B^0\bar{B}^0$ Mixing Correction	no	no	yes	no
Sensitivity to initial state radiation and cm energy	weak	strong	$2\times A_{LR}$	$\sim$weak
Relative sample size needed for equal stat. precision	1 $\mathcal{P}_e = 65\%$	$\sim$150	$\sim$60	$\sim$200

The left-right asymmetry is measured by counting nearly all Z decay modes (e^+e^- final states are excluded) for each of the two longitudinal polarization states of the electron beam. The measurement requires knowledge of the absolute beam polarization, but does not require knowledge of the absolute luminosity, detector acceptance, or efficiency. The properties of the measured asymmetry (A_{LR}^{raw}) are contrasted with those of the other Z pole asymmetries in Table XVIII. Assuming a beam polarization of 65%, the measurement of A_{LR} has 60–200 times more statistical power and is more precise systematically than measurements of the other observables.

In 1992, the SLAC Linear Collider (SLC) was first operated with a polarized electron beam. During that run, the SLD accumulated approximately 10,000 Z events with an average beam polarization of 22%. In 1993, the SLC performance was improved substantially, and a newly-developed strained lattice GaAs cathode[32] has greatly improved the degree of beam polarization. Approximately 50,000 events were accumulated with an average beam polarization larger than 60%.

The technique used to measure A_{LR} is quite straightforward. A simple calorimeter-based analysis isolates hadronic and $\tau^+\tau^-$ final states. Electron pair final states are excluded to avoid contamination from the large t-channel γ-exchange subprocess. Since the electron beam helicity is changed randomly on each machine pulse, the left- and right-handed luminosities are quite similar. The measured asymmetry is formed from the number of events produced with

Table XIX

The systematic uncertainties that affected polarization measurement in 1992 and preliminary values for the 1993 run.

Systematic Uncertainty	$\delta\mathcal{P}_e/\mathcal{P}_e$(1992)	$\delta\mathcal{P}_e/\mathcal{P}_e$(1993)
Laser Polarization	2.0%	$\lesssim$1.5%
Analyzing Power Calibration	0.4%	0.5%
Detector Linearity	1.5%	$\sim$0.7%
Interchannel Consistency	0.9%	0.5%
Electronic Noise Correction	0.4%	0.5%
Total Systematic Uncertainty	2.7%	$\lesssim$1.8%

left-handed electron beam N_L and the number produced with right-handed beam N_R,

$$A_{LR}^{raw} = \frac{N_L - N_R}{N_L + N_R}. \tag{28}$$

The measured asymmetry A_{LR}^{raw} is related to A_{LR} by the following expression which incorporates a number of small correction terms in square brackets:

$$A_{LR} = \frac{A_{LR}^{raw}}{\mathcal{P}_e} + \frac{1}{\mathcal{P}_e}\left[A_{LR}^{raw} f_b + (A_{LR}^{raw})^2 A_{\mathcal{P}} - E_{cm}\frac{\sigma'(E_{cm})}{\sigma(E_{cm})}A_E - A_\varepsilon - A_{\mathcal{L}}\right], \tag{29}$$

where $\mathcal{P}_e$ is the luminosity-weighted average beam polarization; f_b is the background fraction; $\sigma(E)$ is the unpolarized Z cross section at energy E; $\sigma'(E)$ is the derivative of the cross section with respect to E; and $A_{\mathcal{P}}$, A_E, A_ε, and $A_{\mathcal{L}}$ are the left-right asymmetries of the beam polarization, the center-of-mass energy, the product of detector acceptance and efficiency, and the integrated luminosity, respectively.

The dominant systematic error on the A_{LR} determination is the uncertainty on the beam polarization measured by the SLD Compton polarimeter. The various contributions to the 1992 and preliminary 1993 systematic polarization uncertainties are listed in Table XIX.

The 1992 and preliminary 1993 values of the various corrections to A_{LR}^{raw} that are defined in Eq. (29) are listed in Table XX. Note that the 1993 luminosity asymmetry is measured directly using a new high-statistics monitor that detects forward-radiative Bhabha scattering events.

In 1993, the SLC was operated with a flat electron beam. The vertical beam size of 0.9 μm may have been limited by chromatic aberrations. If this were the case, then the luminosity-weighted beam energy might differ from the average beam energy. Since the direction of the beam polarization vector at

Table XX

Corrections to A_{LR} for the 1992 measurement along with preliminary values for the 1993 measurement.

Correction	$\delta A_{LR}/A_{LR}(\%)$ 1992	$\delta A_{LR}/A_{LR}(\%)$ 1993
Background (f_b)	<1.4	0.6±0.3
L-R Polarization Asymmetry ($A_{\mathcal{P}}$)	0.006	0.018±0.030
L-R Energy Asymmetry (A_E)	−0.07	−0.01
L-R Efficiency Asymmetry (A_ε)	∼0	∼0
L-R Luminosity Asymmetry ($A_{\mathcal{L}}$)	0.8±1.9	0.2±0.03
Total Correction	0±2.4	0.8±0.3

the SLC interaction point is correlated with the beam energy, this leads to the possibility that the luminosity-weighted polarization might differ from the average beam polarization measured by the Compton polarimeter. Extensive measurements of the polarization-energy correlation and the machine energy spread have led to the conclusion that the difference between the average beam polarization and the luminosity-weighted quantity is less than 1%. The same studies indicate that the spin transmission of the SLC arc is larger than previously thought ($\gtrsim$95%). Unfortunately, this puts the beam polarization measured by the Compton polarimeter into disagreement with the polarization measured in the linac by a diagnostic Møller polarimeter. As this document is being written, a number of tests are in progress. Until they are complete, no preliminary result from the 1993 run will be available.

The value of A_{LR} measured in 1992 and the preliminary errors on the 1993 result are as follows:

$$\begin{aligned} A_{LR}(91.55\text{ GeV}) &= 0.100 \pm 0.044 \pm 0.004 \quad (1992), \\ A_{LR}(91.28\text{ GeV}) &= \qquad\quad \pm 0.007 \pm 0.003 \quad (1993). \end{aligned}$$

Applying very small corrections for Z-γ interference arising from operation at off-pole energies and initial state radiation, these results can be expressed in terms of $\sin^2\theta_W^{\text{eff}}$,

$$\sin^2\theta_W^{\text{eff}} = \begin{cases} 0.2378 \pm 0.0056 \pm 0.0005 & (1992) \\ \qquad\quad \pm 0.0009 \pm 0.0004 & (1993). \end{cases}$$

4.7 Determination of $\sin^2\theta_W^{\rm eff}$

We should note that the procedures used to extract the various Z-pole asymmetries do contain some Standard Model bias. In all cases, corrections for electroweak interference are applied. The approximate sizes of these corrections are as follows: A_{FB}^{ℓ} (100%), A_{FB}^{c} (15%), A_{FB}^{b} (4.5%), and $\mathcal{P}_\tau/A_{LR}$ (2.8%). Within the context of the MSM, these corrections are largely tree-level and can be applied without much bias to the loop-level tests. However, we are definitely allowing ourselves to be guided by MSM expectations. Should deviations from the MSM appear, these assumptions may require modification.

The use of the parameter $\sin^2\theta_W^{\rm eff}$ to characterize the neutral-current couplings of the various fermions is an MSM-inspired assumption that is amenable to test. Using Eqs. (18) and (19), values of $\sin^2\theta_W^{\rm eff}$ are extracted from the measured values of all of the Z-pole asymmetries and are listed in Table XXI. Note that the different techniques yield remarkably self-consistent results. Assuming that the various electroweak corrections have not caused undue bias, it does appear that it is possible to characterize the ratio of vector and axial vector couplings to the Z with a single parameter. The combined result, $\sin^2\theta_W^{\rm eff} = 0.2321 \pm 0.0006$, is currently the most precise of the electroweak tests. The corresponding 68% confidence region in S-T space is shown in Fig. 9. Note that it occupies less area than any of the confidence regions that we've plotted previously.

4.8 $Zb\bar{b}$ Vertex

The corrections to the $Zb\bar{b}$ vertex differ somewhat from those that affect the lighter quark vertices. The effect of the top quark, which leads to larger m_t-dependent effects, is unsuppressed by CKM factors. Extensions to the MSM which contain mass-dependent couplings can also produce significant effects upon the vertex. The most sensitive test of these corrections is the measurement of the ratio Γ_{bb}/Γ_{had}. This work is described in the presentation of W. Venus at this Symposium.[33]

4.9 Interpretation of Loop-Level Tests

As was discussed at the beginning of this chapter, there are two approaches to the testing of the MSM. The first is to fit the MSM to all observations and to examine the goodness-of-fit. The second is to fit a more general parameterization of the loop-level corrections to the data. The results can then be compared with the predictions of the MSM.

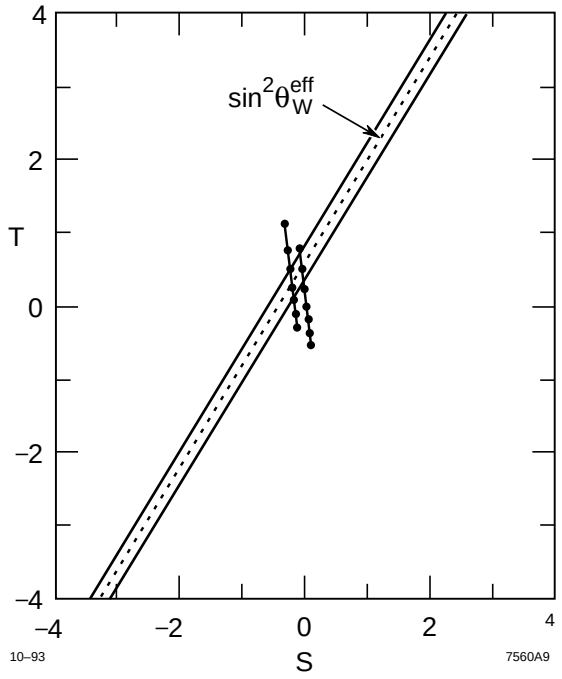

Figure 9. The 68% confidence region in S-T space that corresponds to the measured value of $\sin^2\theta_W^{\rm eff}$. The vertical contours show the MSM predictions for m_H values of 60 GeV and 1000 GeV. The dots indicate various top quark masses between 75 GeV (bottom) and 225 GeV (top) in units of 25 GeV.

Table XXI

A summary of all measurements that determine $\sin^2\theta_W^{\rm eff}$.

Observable	Number of Meas.	$\sin^2\theta_W^{\rm eff}$
$A_{FB}^{\ell,0}$	4	0.2318±0.0010
A_τ	4	0.2325±0.0018
A_e	2	0.2337±0.0032
$A_{FB}^{b,0}$	6	0.2322±0.0011
$A_{FB}^{c,0}$	6	0.2313±0.0036
Q_{FB}	3	0.2320±0.0016
LEP Average	25	0.2321±0.0006
χ^2/dof		0.5/5
A_{LR}	1 (1992 only)	0.2378±0.0056
World Average	26	0.2322±0.0006
χ^2/dof		1.5/6

Table XXII

The measured observables used by the LEP Collaborations[27] in their analysis of the MSM.

Observable	Measurement
LEP Results	
M_Z (GeV)	91.187±0.007
Γ_Z (GeV)	2.489±0.007
σ_0 (nb)	41.56±0.14
R_ℓ	20.763±0.049
$A_{FB}^{\ell,0}$	0.0158±0.0018
+ correlation matrix	
A_τ	0.0139±0.014
A_e	0.0130±0.025
$A_{FB}^{b,0}$	0.099±0.006
$A_{FB}^{c,0}$	0.075±0.015
Γ_{bb}/Γ_{had}	0.2200±0.0027
$\sin^2\theta_W^{\rm eff}$ from Q_{FB}	0.2320±0.0016
$p\bar{p}$ and νN Results	
M_W/M_Z	0.8813±0.0041[21]
M_W (GeV)	79.91±0.39[21]
$1 - M_W^2/M_Z^2$	0.2256±0.0047[25,35]

4.9.1 The MSM Hypothesis

The LEP Collaborations[27] have performed a fit of the MSM (using the computer codes ZFITTER[24] and BHM[34]) to the measured observables listed in Table XXII (they incorporate the LEP lineshape parameter correlation matrix which is reproduced in Appendix A).

Since the dependence of the loop-level corrections on m_H is quite weak, the data do not constrain the Higgs mass to a physically interesting confidence interval. Therefore, the fit is performed with m_H fixed to the values 60 GeV, 300 GeV, and 1000 GeV. The quantities m_t and α_s are allowed to vary as free parameters. The fit is performed on the LEP measurements alone and upon a combination of the LEP results and measurements from hadron collider and neutrino experiments (see Table XXII). The results are summarized in Table XXIII. Note that the central value of each confidence interval refers to the $m_H = 300$ GeV fit. The variation of the result with Higgs mass is presented as the second set of errors in each case.

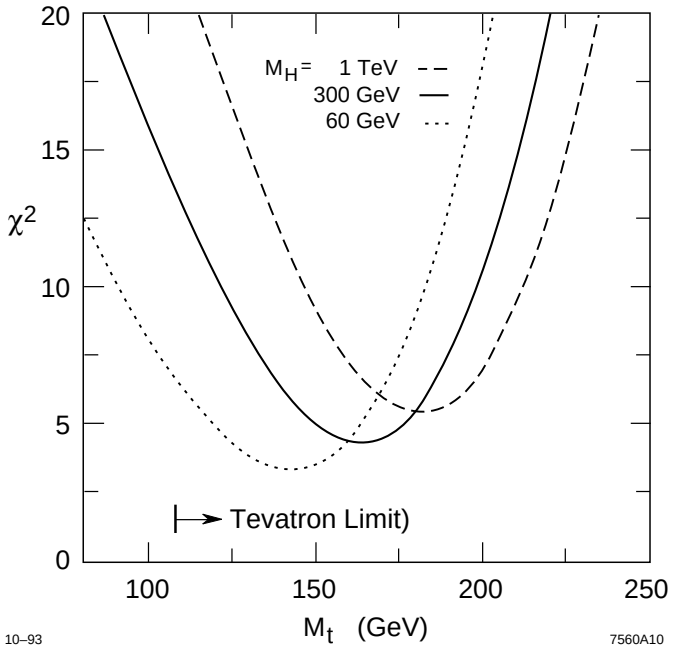

Figure 10. The value χ^2 for the combined fit of the LEP Collaborations[27] (column three in Table XXIII) is plotted as a function of m_t for three values of m_H.

Table XXIII

The results of the MSM fit to all observables performed by the LEP Collaborations.[27]

Parameter	LEP Measurements	LEP Measurements + Collider and ν data
m_t (GeV)	166^{+17+19}_{-19-22}	164^{+16+18}_{-17-21}
$\alpha_s(M_Z^2)$	$0.120\pm0.006\pm0.002$	$0.120\pm0.006\pm0.002$
χ^2/dof	3.5/8	4.4/11
$\sin^2\theta_W^{\rm eff}$	$0.2324\pm0.0005^{+0.0001}_{-0.0002}$	$0.2325\pm0.0005^{+0.0001}_{-0.0002}$
$1-M_W^2/M_Z^2$	$0.2255\pm0.0019^{+0.0005}_{-0.0003}$	$0.2257\pm0.0017^{+0.0004}_{-0.0003}$
M_W (GeV)	$80.25\pm0.10^{+0.02}_{-0.03}$	$80.24\pm0.09^{+0.01}_{-0.02}$

It is clear that the MSM describes all observations quite well. The best estimates of m_t and α_s are 164^{+16+18}_{-17-21} GeV and $0.120\pm0.006\pm0.002$, respectively. The value χ^2 for the combined fit (column three in Table XXIII) is plotted as a function of m_t for each m_H value in Fig. 10. Note that the data have a small (but not significant) preference for smaller m_H values.

Table XXIV

The results of S, T, V fits to all observables.

Parameter	α_s constrained (0.123±0.006)	α_s free
S	−0.45±0.31	−0.44±0.31
T	−0.05±0.32	−0.03±0.33
V	−0.001±0.004	−0.003±0.006 ($\alpha_s = 0.120 \pm 0.006$)
χ^2/dof	3.0/10	2.9/9

4.9.2 The S, T, V Analysis

We can now fit all of the observables that have been discussed in this chapter to common values of S, T, and V. Using the correlation matrix for the LEP lineshape parameters (see Appendix A), an S, T, V fit was performed to the measurements of M_W/M_Z, R_ν, Q_W, Γ_Z, R_ℓ, σ_0, $A_{FB}^{\ell,0}$, A_τ, A_e, $A_{FB}^{b,0}$, $A_{FB}^{c,0}$, and $\sin^2\theta_W^{\rm eff}$ (Q_{FB}). The fits were performed with α_s constrained to the value extracted from QCD measurements,[20] 0.123±0.006, and with α_s (V) as a completely free parameter. The results are listed in Table XXIV.⋆

In order to display the result in S-T space, the parameter probability distribution is integrated over all values of V. This is equivalent to a contraction of the 3×3 inverse parameter covariance matrix to a 2×2 matrix (see Appendix B for details). The 68% and 90% confidence regions that correspond to the α_s-free fit are shown in Fig. 11. Although the central value of S is *unphysical* in the MSM sense, it is clear that the fit is consistent with the MSM contours. It is also clear that the data favor a more negative value of S (which corresponds to a lighter Higgs boson).

The consistency of the measured S-T confidence region and the MSM contours can be quantified by performing a fit of the contour functions $S(m_t, m_H)$ and $T(m_t, m_H)$ to the measured ellipses. The Higgs mass is fixed to 60 GeV, 300 GeV, 1000 GeV, and the top mass is allowed to vary as a free parameter. The results of these fits are summarized in Table XXV. The fit probabilities are excellent in all cases. Again, it is clear that lighter Higgs bosons are preferred but not significantly. The central values of the m_t confidence intervals agree well with the full MSM fits performed by LEP Collaborations. Note however, that the m_t uncertainties are substantially smaller than those associated with the MSM fits.

⋆ The results presented at the Symposium were based on an MSM calculation of the reference values that did not include order $\alpha\alpha_s$ corrections. The resulting value of V was somewhat more negative.

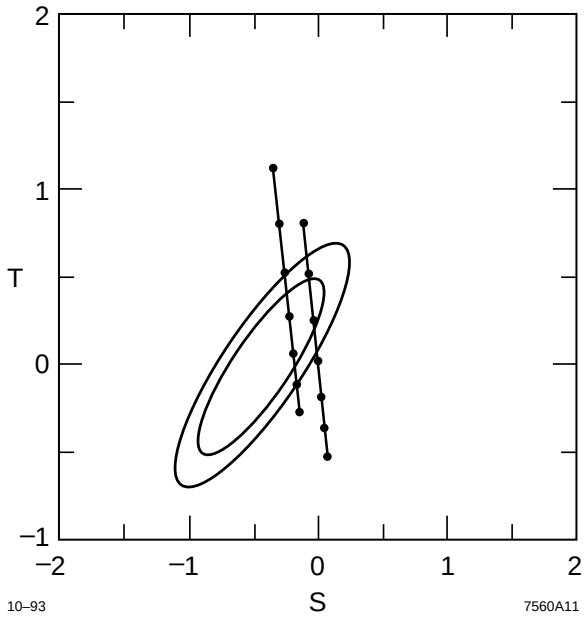

Figure 11. The 68% and 90% confidence regions in S-T space that result from the α_s-free fit to all observables. The vertical contours show the MSM predictions for m_H values of 60 GeV and 1000 GeV. The dots indicate various top quark masses between 75 GeV (bottom) and 225 GeV (top) in units of 25 GeV.

Table XXV

The results of MSM fits to the measured S-T ellipses.

	α_s constrained		α_s free	
m_H (GeV)	m_t (GeV)	$P(\chi^2)$	m_t (GeV)	$P(\chi^2)$
60	146^{+12}_{-13}	56%	148^{+13}_{-14}	84%
300	166±12	44%	167^{+12}_{-13}	46%
1000	182^{+11}_{-12}	29%	184±12	31%

The small m_t confidence intervals are a consequence of the fact that the S-T fits prefer an *unphysical* (in the MSM sense) region of S-T space. It is clear that true MSM fits (which implicitly constrain S and T to an MSM contour) are needed to estimate MSM parameters.

5. Concluding Remarks

1. The Minimal Electroweak Standard Model continues to resist our attempts to finds its cracks. The precision of current electroweak tests is now comparable to the magnitude of purely weak corrections, and no deviations from the MSM are yet apparent.
2. The LEP experiments have measured the S-T trajectories corresponding to Γ_Z ($m^{ST} = 0.37$) and $\sin^2\theta_W^{\rm eff}$ ($m^{ST} = 1.4$) very precisely. In the near future, the uncertainty on Γ_Z should improve from 7 MeV to some value in the neighborhood of 3 MeV. The uncertainty on the $\sin^2\theta_W^{\rm eff}$ trajectory should benefit from the new measurement of A_{LR} by SLD and from continued progress at LEP.
3. New measurements of M_W by the CDF and D0 Collaborations should improve the constraints on the $m^{ST} = 0.65$ trajectory in near future. (They should also provide important information on the U parameter.)
4. The *discovery* of the t quark and the subsequent measurement of its mass will greatly improve the power of the MSM tests. An additional benefit will be that the business of precision electroweak testing can escape (somewhat) from the shadow of parameter estimation and be recognized for what it is, *the testing of the Electroweak Standard Model*. So to our Tevatron colleagues, please hurry!

5.0.1 Acknowledgements:

By definition, a reviewer cannot review without submitted work. I would like to thank the many contributors who made the considerable effort to supply me with interesting things to say (however, please make your submissions more promptly the next time). Unfortunately, time and space limitations prevent me from including all submitted papers. Please forgive me if you do not find your work included in this review. I would like to thank Dorothee Schaile and her colleagues in the LEP Electroweak Working Group for their remarkable compilation and combination of LEP results. They condensed a cubic meter of paper documents into an extremely useful 30 page summary. Finally, Michael Peskin deserves special thanks for his helpful conversations, his assistance with various technical aspects of the S-T analysis, and his comments on this document. This work was supported by the Department of Energy, contract DE-AC03-76SF00515.

REFERENCES

1. See the presentation of S. Chivukula at this Symposium.
2. E.R. Cohen and B.N. Taylor, *Rev. Mod. Phys.* **59**, 1121 (1987).
3. *Review of Particle Properties*, K. Hikasa *et al.*, *Phys. Rev.* **D45**, Part II (1992).
4. CERN–PPE/93–53, March 1993.
5. M. Consoli and W. Hollik, *Z Physics at LEP I*, Geneva, Switzerland, edited by G. Altarelli, R. Kleiss, and C. Verzegnassi, CERN–89–08 1989.
6. CDF Collaboration: paper submitted to this Symposium.
7. D0 Collaboration: S. Abachi *et al.*, paper submitted to this Symposium.
8. A.D. Martin, W.J. Stirling, and R.G. Roberts, *Phys. Lett.* **B228**, 149 (1989).
9. D0 calculation based upon R. Hamberg, W.L. van Neerven, and T. Matsuura, *Nucl. Phys.* **B359**, 343 (1989).
10. UA2 Collaboration: R. Ansari *et al.*, *Phys. Lett.* **B194**, 158 (1987) and CDF Collaboration: F. Abe *et al.*, *Phys. Rev. Lett.* **64**, 152 (1990).
11. CDF Collaboration: F. Abe *et al.*, FERMILAB–CONF–93–211–E, August 1993.
12. L3 Collaboration: O. Adriani *et al.*, CERN–PPE/93–44, March 1993.
13. Z' due to extended gauge groups: R.W. Robinett, *Phys. Rev.* **D26**, 2388 (1982); R.W. Robinett, J.L. Rosner, *Phys. Rev.* **D26**, 2396 (1982); D. London, J.L. Rosner, *Phys. Rev.* **D34**, 1530 (1986); G. Belanger, S. Godfrey, *Phys. Rev.* **D35**, 378 (1987); Z' due in L-R symmetric models: R.W. Robinett, J.L. Rosner, *Phys. Rev.* **D25**, 3036 (1982) and erratum *Phys. Rev.* **D27**, 679 (1982); C. Leung, J.L. Rosner, *Phys. Rev.* **D29**, 2132 (1982).
14. M. Peskin, private communication.
15. K.T. Mahanthappa and P.K. Mohapatra, *Phys. Rev.* **D42**, 1732 and 2400 (1990); F. del Aguila, W. Hollik, J.M. Mozens, and M. Quiros, *Nucl. Phys.* **B372**, 3 (1992); J. Layssac, F.M. Renard, and C. Verzegnassi, *Phys. Lett.* **B287**, 267 (1992).
16. M.E. Peskin and T. Takeuchi, *Phys. Rev. Lett.* **65**, 964 (1990), and *Phys. Rev.* **D46**, 381 (1992).
17. W.J. Marciano and J.L. Rosner, *Phys. Rev. Lett.* **65**, 2963 (1990).
18. D.C. Kennedy and P.G. Langacker, *Phys. Rev. Lett.* **65**, 2967 (1990).
19. G. Altarelli, and R. Barbieri *Phys. Lett.* **B253**, 161 (1991) and G. Altarelli, R. Barbieri, and S. Jadach, *Nucl. Phys.* **B369**, 3 (1992).

20. S. Bethke, Proceedings of the Linear Collider Workshop in Waikoloa, HI, April 1993.

21. UA2 Collaboration: J. Alitti, *et al.*, *Phys. Lett.* **B276**, 354 (1992) and CDF Collaboration: F. Abe, *et al.*, *Phys. Rev. Lett.* **65**, 2243 (1990);

22. The value listed in Table V is taken from an average by G. Altarelli, R. Barbieri, and F. Caravaglios, CERN–TH–6859/93, April 1993.

23. M.C. Noecker, B.P. Masterson, and C.E. Weiman, *Phys. Rev. Lett.* **61**, 310 (1988); S.A. Blundell, W.R. Johnson, and J. Sapirstein, *Phys. Rev. Lett.* **65**, 1411 (1990).

24. We use the ZFITTER package to compute the reference values of all observables used in our S-T analysis. See D. Bardin *et al.*, CERN–TH–6443–92, May 1992.

25. CDHS Collaboration: A. Blondel *et al.*, *Z. Phys.* **C45**, 361 (1990).

26. See for example, R. Stuart, *Z. Phys.* **C34**, 445 (1987).

27. The LEP Collaborations: ALEPH, DELPHI, L3, OPAL, and the LEP Electroweak Working Group, CERN–PPE/93–157, August 1993.

28. D. Buskulic *et al.*, CERN–PPE/93–39, March 1993.

29. T. Sjostrand, CERN–TH–6488–92, May 1992.

30. Unfortunately, a description of the improved measurement is not currently available.

31. K. Abe, *et al.*, *Phys. Rev. Lett.* **70**, 2515 (1993).

32. T. Maruyama, E.L. Garwin, R. Prepost, and G. Zapalac, *Phys. Rev.* **B46**, 4261 (1992).

33. See the presentation of W. Venus at this Symposium.

34. G. Burgers, W. Hollik, and M. Martinez; M. Consoli, W Hollik, and F. Jegerlehner: Proceedings of the Workshop on Z Physics at LEP I, CERN 89–08 Vol. I, 7; and G. Burgers, F. Jegerlehner, B. Kniehl, and A. Sirlin, ibid., 55.

35. CHARM Collaboration: J.V. Allaby *et al.*, *Z. Phys.* **C36**, 611 (1987); CCFR Collaboration: B. King *et al.*, NEVIS–1489, MARCH 1993.

APPENDIX A: LEP Lineshape Parameter Correlation Matrices

Table XXVI

The correlation matrix for the LEP total nine-parameter fit [27] given in Table VIII.

	M_Z	Γ_Z	σ_0	R_e	R_μ	R_τ	$A_{FB}^{e,0}$	$A_{FB}^{\mu,0}$	$A_{FB}^{\tau,0}$
M_Z	1.000	–0.157	0.006	0.029	–0.002	–0.003	0.025	0.056	0.048
Γ_Z	–0.157	1.000	–0.070	0.001	0.006	–0.001	0.000	0.004	0.006
σ_0	0.006	–0.070	1.000	0.071	0.100	0.085	0.008	–0.002	–0.001
R_e	0.029	0.001	0.071	1.000	0.102	0.072	–0.023	0.021	0.018
R_μ	–0.002	0.006	0.100	0.102	1.000	0.076	–0.001	0.007	–0.002
R_τ	–0.003	–0.001	0.085	0.072	0.076	1.000	0.000	–0.002	0.006
$A_{FB}^{e,0}$	0.025	0.000	0.008	–0.023	–0.001	0.000	1.000	–0.062	–0.048
$A_{FB}^{\mu,0}$	0.056	0.004	–0.002	0.021	0.007	–0.002	–0.062	1.000	0.119
$A_{FB}^{\tau,0}$	0.048	0.006	–0.001	0.018	–0.002	0.006	–0.048	0.119	1.000

Table XXVII

The correlation matrix for the LEP total five-parameter fit [27] given in Table IX.

	M_Z	Γ_Z	σ_0	R_ℓ	$A_{FB}^{\ell,0}$
M_Z	1.000	−0.157	0.007	0.012	0.075
Γ_Z	−0.157	1.000	−0.070	0.003	0.006
σ_0	0.007	−0.070	1.000	0.137	0.003
R_ℓ	0.012	0.003	0.137	1.000	0.008
$A_{FB}^{\ell,0}$	0.075	0.006	0.003	0.008	1.000

APPENDIX B: The V Integration

The confidence intervals of the three-parameter fit for S, T, and V are derived in the usual way from an expansion of χ^2 about its minimum in parameter space. Denoting the parameters as $A_i = (S, T, V)$ and the minimum point as $A_i^* = (S^*, T^*, V^*)$, the χ^2 expansion is given by the following expression:

$$\begin{aligned} \chi^2 &= \chi^2(A^*) + \frac{1}{2}\frac{\partial^2\chi^2}{\partial A_i \partial A_j}\bigg|_{A^*}(A_i - A_i^*)(A_j - A_j^*) \\ \chi^2 &= \chi^2(A^*) + C_{ij}(A_i - A_i^*)(A_j - A_j^*), \end{aligned} \tag{30}$$

where C_{ij} is the inverse parameter covariance matrix. The usual single-parameter confidence intervals are found by integrating the χ^2 probability,

$$dP = \text{const} \cdot e^{-\chi^2/2} dA_1 dA_2 dA_3, \tag{31}$$

over two of the parameters. The RMS of the remaining Gaussian distribution has the familiar form $\sigma_i = \sqrt{(C^{-1})_{ii}}$ where C^{-1} is the inverse of C. However to obtain the equation of the S-T ellipse, we wish to integrate Eq. (31) over A_3 only. The resulting Gaussian distribution can be represented as the reduced χ^2,

$$\bar{\chi}^2 = \chi^2(A^*) + \bar{C}_{ij}(A_i - A_i^*)(A_j - A_j^*), \tag{32}$$

where the reduced inverse covariance matrix $\bar{C}$ is given by the following simple expression:

$$\begin{aligned} \bar{C}_{11} &= C_{11} - \frac{C_{13}C_{31}}{C_{33}} \\ \bar{C}_{12} &= C_{12} - \frac{C_{13}C_{32}}{C_{33}} \\ \bar{C}_{22} &= C_{22} - \frac{C_{23}C_{32}}{C_{33}}. \end{aligned} \tag{33}$$

Equations (32) and (33) define the two-dimensional ellipses that are plotted in Fig. 11.

Table of Contents